

1                   Quasi-consistent efficient meshfree thin shell  
2                   formulation to naturally accommodate essential  
3                   boundary conditions

4                   Junchao Wu<sup>a,\*</sup>, Yangtao Xu<sup>b</sup>, Bin Xu<sup>a</sup>, Syed Humayun Basha<sup>c,\*</sup>

<sup>a</sup>*Key Laboratory for Intelligent Infrastructure and Monitoring of Fujian Province, College  
of Civil Engineering, Huaqiao University, Xiamen, Fujian, 361021, China*

<sup>b</sup>*College of Civil Engineering, Huaqiao University, Xiamen, Fujian, 361021, China*

<sup>c</sup>*Key Laboratory for Structural Engineering and Disaster Prevention of Fujian Province,  
College of Civil Engineering, Huaqiao University, Xiamen, Fujian, 361021, China*

---

5   **Abstract**

This research proposed an efficient and quasi-consistent meshfree thin shell formulation with natural enforcement of essential boundary conditions. Within the framework of the Hu-Washizu variational principle, a mixed formulation of displacements, strains and stresses is employed in this approach, where the displacements are discretized using meshfree shape functions, and the strains and stresses are expressed using smoothed gradients, covariant smoothed gradients and covariant bases. The smoothed gradients satisfy the first and second order integration constraint and have quasi-consistent consistency. Owing to Hu-Washizu variational principle, the essential boundary conditions automatically arise in its weak form. As a result, the suggested technique's enforcement of essential boundary conditions resembles that of the traditional Nitsche's method. Contrary to Nitsche's method, the costly higher order derivatives of conventional meshfree shape functions were replaced by the smoothed gradients with fast computation, which improve the efficiency. Meanwhile, the proposed formulation features a naturally stabilized term without adding any artificial stabilization factors, which eliminates the stabilization parameter-dependent issue in the Nitsche's method. The efficacy of the proposed Hu-Washizu meshfree thin shell formulation is illustrated by a set of classical standard thin shell problems.

6   *Keywords:* Meshfree, Thin shell, Hu-Washizu variational principle,  
7   Reproducing kernel gradient smoothing, Essential boundary condition

---

---

\*Corresponding author

*Email addresses:* jcwu@hqu.edu.cn (Junchao Wu), syedhbasha@hqu.edu.cn (Syed Humayun Basha)

## 8 1. Introduction

9 Thin shell structures generally adhere to the Kirchhoff hypothesis [1], that  
10 neglects the shear deformation can be described using Galerkin formulation  
11 which requires to have at least  $C^1$  continuity. The traditional finite element  
12 methods usually only have  $C^0$  continuous shape functions, and it prefers Mindlin  
13 thick shear theory, hybrid and mixed models in simulation of shell structure [2].  
14 Meshfree methods [3, 4, 5] with high order smoothed shape functions have gar-  
15 nered much research attention over the past thirty years. These techniques  
16 established the shape functions based on a collection of dispersed nodes, and  
17 the high order continuity of shape functions can be easily achieved even with  
18 low-order basis functions. For thin shell analysis, this high order meshfree ap-  
19 proximation can also alleviate the membrane locking caused by the mismatched  
20 approximation order of membrane strain and bending strain [6]. Furthermore,  
21 nodal-based meshfree approximations generally offer the flexibility of local re-  
22 finement and can relieve the burden of mesh distortion. Owing to these benefits,  
23 numerous meshfree techniques have been developed and implemented in many  
24 scientific and engineering fields [7, 8, 9, 10, 11, 12]. However, the high order  
25 smoothed meshfree shape functions accompany the enlarged and overlapping  
26 supports, which may potentially cause many problems for shape functions. One  
27 of the issues is the loss of the Kronecker delta property, which means that, un-  
28 like the finite element methods, the necessary boundary conditions cannot be  
29 directly enforced [13]. Another issue is that the variational consistency or said  
30 integration constraint cannot be satisfied due to the misalignment between the  
31 numerical integration domains and supports of shape functions. Besides, the  
32 shape functions exhibit a piecewise rational nature in each integration domain.  
33 Therefore, variational consistency is vital to the solution accuracy in Galerkin  
34 formulations [14, 15].

35 Various ways have been presented to enforce the necessary boundary for  
36 Galerkin meshfree methods directly, including the boundary singular kernel  
37 method [16], mixed transformation method [16], and interpolation element-free  
38 method [17] for recovering shape functions' Kronecker property. However, these  
39 methods are not based on a variational setting and cannot guarantee varia-  
40 tional consistency. In the absence of a meshfree node, accuracy enforcement  
41 might be poorer. In contrast, enforcing the essential boundary conditions using  
42 a variational approach is preferred for Galerkin meshfree methods. The varia-  
43 tional consistent Lagrange multiplier approach was initially used to the Galerkin  
44 meshfree method by Belytschko et al. [3]. In this method, the extra degrees  
45 of freedom are used to determine the discretion of Lagrange multiplier. Fur-  
46 thermore, Ivannikov et al. [18] have extended this approach to geometrically  
47 nonlinear thin shells. Lu et al. [19] suggested the modified variational es-  
48 sential boundary enforcement approach and expressed the Lagrange multiplier  
49 by equivalent tractions to eliminate the excess degrees of freedom. However,  
50 the coercivity of this approach is not always ensured and potentially reduces  
51 the accuracy. Zhu and Atluri [20] pioneered the penalty method for meshfree  
52 method, making it a straightforward approach to enforce essential boundary

53 conditions via Galerkin weak form. However, the penalty method lacks varia-  
 54 tional consistency and requires experimental artificial parameters whose optimal  
 55 value is hard to determine. Fernández-Méndez and Huerta [13] imposed neces-  
 56 sary boundary conditions using Nitsche’s approach in the meshfree formulation.  
 57 This approach can be seen as a hybrid combination of the modified variational  
 58 method and the penalty method because the modified variational method gen-  
 59 erates variational consistency through the use of a consistent term, and the  
 60 penalty method is used as a stabilized term to recover the coercivity. Skatulla  
 61 and Sansour [21] extended Nitsche’s thin shell analysis method and proposed an  
 62 iteration algorithm to determine artificial parameters at each integration point.

63 In order to address the issue of numerical integration, a series of consis-  
 64 tent integration schemes have been developed for Galerkin meshfree methods.  
 65 Among these include stabilized conforming nodal integration [22], variational  
 66 consistent integration [23], quadratic consistent integration [24], reproducing  
 67 kernel gradient smoothing integration [25], and consistent projection integration  
 68 [26]. The assumed strain approach establishes the most consistent integration  
 69 scheme, while the smoothed gradient replaces the costly higher order derivatives  
 70 of traditional meshfree shape functions and shows a high efficiency. Moreover,  
 71 to achieve global variational consistency, a consistent essential boundary con-  
 72 dition enforcement should cooperate with the consistent integration scheme.  
 73 The consistent integration scheme and Nitsche’s method for treating essential  
 74 boundary conditions show a good performance since they can satisfy the coer-  
 75 civity without requiring additional degrees of freedom. Nevertheless, Nitsche’s  
 76 approach still retains the artificial parameters in stabilized terms, and it is es-  
 77 sential to remain conscious of the costly higher order derivatives, particularly  
 78 for thin plate and thin shell problems. Recently, Wu et al. [27, 28] proposed  
 79 an efficient and stabilized essential boundary condition enforcement method  
 80 based upon the Hellinger-Reissner variational principle, where a mixed formu-  
 81 lation in Hellinger-Reissner weak form recasts the reproducing kernel gradient  
 82 smoothing integration. The terms for enforcing essential boundary conditions  
 83 are identical to the Nitsche’s method, and both have consistent and stabilized  
 84 terms. Nevertheless, the stabilized term of this method naturally exists in the  
 85 Hellinger-Reissner weak form and no longer needs the artificial parameters, even  
 86 for essential boundary enforcement; instead all of the higher order derivatives  
 87 are represented by smoothed gradients and their derivatives.

88 In this study, an efficient and stabilized variational consistent meshfree  
 89 method that naturally enforces the essential boundary conditions is developed  
 90 for thin shell structure. Following the concept of the Hellinger-Reissner prin-  
 91 ciple base consistent meshfree method, the Hu-Washizu variational principle of  
 92 complementary energy with variables of displacement, strains, and stresses is  
 93 employed. The displacement is approximated by conventional meshfree shape  
 94 functions, and the strains and stresses are expressed by smoothed gradients with  
 95 covariant bases. It is important to note that although the first second-order in-  
 96 tegration requirements are naturally embedded in the smoothed gradients, their  
 97 fulfillment can only result in a quasi-satisfaction of variational consistency be-  
 98 cause of the non-polynomial nature of the stresses. Hu-Washizu’s weak form is

99 used to evaluate all the essential boundary conditions regarding displacements  
100 and rotations. This type of formulation is similar to the Nitsche's method but  
101 does not require any artificial parameters. Compared with Nitsche's method,  
102 conventional reproducing smoothed gradients and its direct derivatives replace  
103 the costly higher order derivatives. By utilizing the advantages of a replicating  
104 kernel gradient smoothing framework, the smoothed gradients showed better  
105 performance compared to conventional derivatives of shape functions, hence  
106 increasing the meshfree formulation's computational efficiency.

107 The remainder of this research paper is structured as follows: The kinematics  
108 of the thin shell structure and the weak form of the associated Hu-Washizu  
109 principle are briefly described in Section 2. Subsequently, the mixed formulation  
110 regarding the displacements, strains and stresses in accordance with Hu-Washizu  
111 weak form are presented in Section 3. The discrete equilibrium equations are  
112 derived in Section 4 using the naturally occurring accommodation of essential,  
113 and they are compared to the equations obtained using Nitsche's method. The  
114 numerical results in Section 5 validate the efficacy of the proposed Hu-Washizu  
115 meshfree thin shell formulation. Lastly, the concluding remarks are presented  
116 in Section 6.

## 117 2. Hu-Washizu's formulation of complementary energy for thin shell

### 118 2.1. Kinematics for thin shell

119 Consider the configuration of a shell  $\bar{\Omega}$ , as shown in Fig. 1, which can be  
 120 easily described by a parametric curvilinear coordinate system  $\boldsymbol{\xi} = \{\xi^i\}_{i=1,2,3}$ .  
 121 The mid-surface of the shell denoted by  $\Omega$  is specified by the in-plane coordinates  
 122  $\boldsymbol{\xi} = \{\xi^\alpha\}_{\alpha=1,2}$ , as the thickness direction of shell is by  $\xi^3$ ,  $-\frac{h}{2} \leq \xi^3 \leq \frac{h}{2}$ ,  $h$  is  
 123 the thickness of shell. In this work, Latin indices take the values from 1 to 3,  
 124 and Greek indices are evaluated by 1 or 2. For the Kirchhoff hypothesis [6], the  
 125 position  $\mathbf{x} \in \bar{\Omega}$  is defined by linear functions with respect to  $\xi^3$  :

$$\mathbf{x}(\xi^1, \xi^2, \xi^3) = \mathbf{r}(\xi^1, \xi^2) + \xi^3 \mathbf{a}_3(\xi^1, \xi^2) \quad (1)$$

in which  $\mathbf{r}$  means the position on the mid-surface of shell, and  $\mathbf{a}_3$  is correspond-

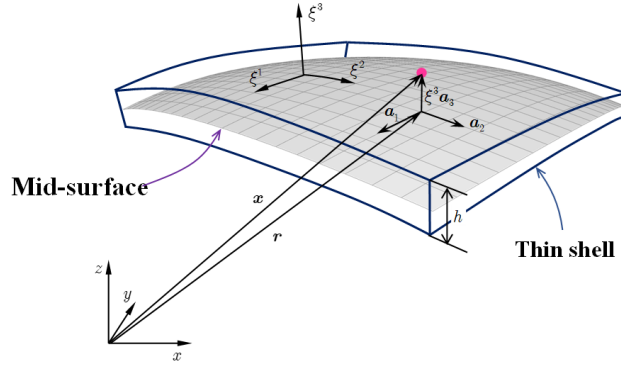


Figure 1: Kinematics for thin shell.

126 ing normal direction. For the mid-surface of shell, the in-plane covariant base  
 127 vector with respect to  $\xi^\alpha$  can be derived by a trivial partial differentiation to  $\mathbf{r}$ :  
 128

$$\mathbf{a}_\alpha = \frac{\partial \mathbf{r}}{\partial \xi^\alpha} = \mathbf{r}_{,\alpha}, \alpha = 1, 2 \quad (2)$$

129 to provide for a clear expression, the subscript comma denotes the partial dif-  
 130 ferentiation operation with respect to in-plane coordinates  $\xi^\alpha$ , and the normal  
 131 vector  $\mathbf{a}_3$  can be obtained by the normalized cross product of  $\mathbf{a}_\alpha$ 's as follows:

$$\mathbf{a}_3 = \frac{\mathbf{a}_1 \times \mathbf{a}_2}{\|\mathbf{a}_1 \times \mathbf{a}_2\|} \quad (3)$$

132 where  $\|\bullet\|$  is the Euclidean norm operator.

133 With the assumption of infinitesimal deformation, the strain components  
 134 with respect to the global contravariant base can be stated as:

$$\epsilon_{ij} = \frac{1}{2}(\mathbf{x}_{,i} \cdot \mathbf{u}_{,j} + \mathbf{u}_{,i} \cdot \mathbf{x}_{,j}) \quad (4)$$

where  $\mathbf{u}$  represents the displacement for the shell deformation. To satisfy the Kirchhoff hypothesis, the displacement is assumed to be of the following form:

$$\mathbf{u}(\xi^1, \xi^2, \xi^3) = \mathbf{v}(\xi^1, \xi^2) + \boldsymbol{\theta}(\xi^1, \xi^2)\xi^3 \quad (5)$$

in which the quadratic and higher order terms are neglected.  $\mathbf{v}$ ,  $\boldsymbol{\theta}$  represent the displacement and rotation in mid-surface, respectively.

Subsequently, plugging Eqs. (1) and (5) into Eq. (4) and neglecting the quadratic terms, the strain components can be rephrased as follows:

$$\begin{aligned} \epsilon_{\alpha\beta} &= \frac{1}{2}(\mathbf{a}_\alpha \cdot \mathbf{v}_{,\beta} + \mathbf{v}_{,\alpha} \cdot \mathbf{a}_\beta) \\ &\quad + \frac{1}{2}(\mathbf{a}_{3,\alpha} \cdot \mathbf{v}_{,\beta} + \mathbf{v}_{,\alpha} \cdot \mathbf{a}_{3,\beta} + \mathbf{a}_\alpha \cdot \boldsymbol{\theta}_{,\beta} + \boldsymbol{\theta}_{,\alpha} \cdot \mathbf{a}_\beta)\xi^3 \\ &= \varepsilon_{\alpha\beta} + \kappa_{\alpha\beta}\xi^3 \end{aligned} \quad (6a)$$

$$\epsilon_{\alpha 3} = \frac{1}{2}(\mathbf{a}_\alpha \cdot \boldsymbol{\theta} + \mathbf{v}_{,\alpha} \cdot \mathbf{a}_3) + \frac{1}{2}(\mathbf{a}_3 \cdot \boldsymbol{\theta})_{,\alpha}\xi^3 \quad (6b)$$

$$\epsilon_{33} = \mathbf{a}_3 \cdot \boldsymbol{\theta} \quad (6c)$$

where  $\varepsilon_{\alpha\beta}$ ,  $\kappa_{\alpha\beta}$  represent membrane and bending strains, respectively, and are given as follows:

$$\varepsilon_{\alpha\beta} = \frac{1}{2}(\mathbf{a}_\alpha \cdot \mathbf{v}_{,\beta} + \mathbf{v}_{,\alpha} \cdot \mathbf{a}_\beta) \quad (7)$$

$$\kappa_{\alpha\beta} = \frac{1}{2}(\mathbf{a}_{3,\alpha} \cdot \mathbf{v}_{,\beta} + \mathbf{v}_{,\alpha} \cdot \mathbf{a}_{3,\beta} + \mathbf{a}_\alpha \cdot \boldsymbol{\theta}_{,\beta} + \boldsymbol{\theta}_{,\alpha} \cdot \mathbf{a}_\beta) \quad (8)$$

In accordance with the Kirchhoff hypothesis, the thickness of shell will not change, and the deformation related with direction of  $\xi^3$  will vanish, i.e.  $\epsilon_{3i} = 0$ . Thus, the rotation  $\boldsymbol{\theta}$  can be rewritten as:

$$\epsilon_{3i} = 0 \Rightarrow \begin{cases} \boldsymbol{\theta} \cdot \mathbf{a}_\alpha + \mathbf{v}_{,\alpha} \cdot \mathbf{a}_3 = 0 \\ \boldsymbol{\theta} \cdot \mathbf{a}_3 = 0 \end{cases} \Rightarrow \boldsymbol{\theta} = -\mathbf{v}_{,\alpha} \cdot \mathbf{a}_3 \mathbf{a}^\alpha \quad (9)$$

where  $\mathbf{a}^\alpha$ 's is the in-plane contravariant base vector,  $\mathbf{a}^\alpha \cdot \mathbf{a}_\beta = \delta^\alpha_\beta$ ,  $\delta$  is the Kronecker delta function. Substituting Eq. (9) into Eq. (8) leads to:

$$\kappa_{\alpha\beta} = (\Gamma_{\alpha\beta}^\gamma \mathbf{v}_{,\gamma} - \mathbf{v}_{,\alpha\beta}) \cdot \mathbf{a}_3 = -\mathbf{v}_{,\alpha}|_\beta \cdot \mathbf{a}_3 \quad (10)$$

in which  $\Gamma_{\alpha\beta}^\gamma = \mathbf{a}_{\alpha,\beta} \cdot \mathbf{a}^\gamma$  is namely the Christoffel symbol of the second kind, and  $\mathbf{v}_{,\alpha}|_\beta$  is the in-plane covariant derivative of  $\mathbf{v}_{,\alpha}$ , i.e.  $\mathbf{v}_{,\alpha}|_\beta = \Gamma_{\alpha\beta}^\gamma \mathbf{v}_{,\gamma} - \mathbf{v}_{,\alpha\beta}$ .

## 2.2. Galerkin weak form for Hu-Washizu principle of complementary energy

In this study, the Hu-Washizu variational principle of complementary energy [29] was adopted for the development of the proposed analytical approach, the

154 corresponding complementary functional, denoted by  $\Pi_C$ , is listed as follows:

$$\begin{aligned}
& \Pi_C(\varepsilon_{\alpha\beta}, \kappa_{\alpha\beta}, N^{\alpha\beta}, M^{\alpha\beta}) \\
&= \int_{\Omega} \frac{h}{2} \varepsilon_{\alpha\beta} C^{\alpha\beta\gamma\eta} \varepsilon_{\gamma\eta} d\Omega + \int_{\Omega} \frac{h^3}{24} \kappa_{\alpha\beta} C^{\alpha\beta\gamma\eta} \kappa_{\gamma\eta} d\Omega \\
&+ \int_{\Omega} \varepsilon_{\alpha\beta} (N^{\alpha\beta} - h C^{\alpha\beta\gamma\eta} \varepsilon_{\gamma\eta}) d\Omega + \int_{\Omega} \kappa_{\alpha\beta} (M^{\alpha\beta} - \frac{h^3}{12} C^{\alpha\beta\gamma\eta} \kappa_{\gamma\eta}) d\Omega \\
&- \int_{\Gamma_v} \mathbf{T} \cdot \bar{\mathbf{v}} d\Gamma + \int_{\Gamma_{\theta}} M_{\mathbf{nn}} \bar{\theta}_{\mathbf{n}} d\Gamma - (P \mathbf{a}_3 \cdot \bar{\mathbf{v}})_{\mathbf{x} \in C_w}
\end{aligned} \tag{11}$$

155 where  $C^{\alpha\beta\gamma\eta}$ 's represent the components of fourth order elasticity tensor with  
156 respect to the covariant base and plane stress assumption, and it can be ex-  
157 pressed by Young's modulus  $E$ , Poisson's ratio  $\nu$  and the in-plane contravariant  
158 metric coefficients  $a^{\alpha\beta}$ 's,  $a^{\alpha\beta} = \mathbf{a}^{\alpha} \cdot \mathbf{a}^{\beta}$ , as follows:

$$C^{\alpha\beta\gamma\eta} = \frac{E}{2(1+\nu)} (a^{\alpha\gamma} a^{\beta\eta} + a^{\alpha\eta} a^{\beta\gamma} + \frac{2\nu}{1-\nu} a^{\alpha\beta} a^{\gamma\eta}) \tag{12}$$

159 and  $N^{\alpha\beta}$ ,  $M^{\alpha\beta}$  are the components of membrane and bending stresses given by:

$$N^{\alpha\beta} = h C^{\alpha\beta\gamma\eta} \varepsilon_{\gamma\eta}, \quad M^{\alpha\beta} = \frac{h^3}{12} C^{\alpha\beta\gamma\eta} \kappa_{\gamma\eta} \tag{13}$$

160 Essential boundaries on the edges and corners denoted by  $\Gamma_v$ ,  $\Gamma_{\theta}$  and  $C_v$  are  
161 naturally existed in complementary energy functional,  $\bar{\mathbf{v}}$ ,  $\bar{\theta}_{\mathbf{n}}$  are the correspond-  
162 ing prescribed displacement and normal rotation, respectively.  $\mathbf{T}$ ,  $M_{\mathbf{nn}}$  and  $P$   
163 can be determined by Euler-Lagrange equations of shell problem [30] as follows:

$$\mathbf{T} = \mathbf{T}_N + \mathbf{T}_M \rightarrow \begin{cases} \mathbf{T}_N = \mathbf{a}_{\alpha} N^{\alpha\beta} n_{\beta} \\ \mathbf{T}_M = (\mathbf{a}_3 M^{\alpha\beta} s_{\alpha} n_{\beta})_{,\gamma} s^{\gamma} + (\mathbf{a}_3 M^{\alpha\beta})|_{\beta} n_{\alpha} \end{cases} \tag{14}$$

$$M_{\mathbf{nn}} = M^{\alpha\beta} n_{\alpha} n_{\beta} \tag{15}$$

$$P = -[[M^{\alpha\beta} s_{\alpha} n_{\beta}]] \tag{16}$$

166 where  $\mathbf{n} = n^{\alpha} \mathbf{a}_{\alpha} = n_{\alpha} \mathbf{a}^{\alpha}$  and  $\mathbf{s} = s^{\alpha} \mathbf{a}_{\alpha} = s_{\alpha} \mathbf{a}^{\alpha}$  are the outward normal and  
167 tangent directions on boundaries.  $[[f]]$  is the jump operator defined by:

$$[[f]]_{\mathbf{x}=\mathbf{x}_c} = \lim_{\epsilon \rightarrow 0^+} (f(\mathbf{x}_c + \epsilon) - f(\mathbf{x}_c - \epsilon)), \mathbf{x}_c \in \Gamma \tag{17}$$

168 where  $f$  is an arbitrary function on  $\Gamma$ .

169 Moreover, the natural boundary conditions should be applied by Lagrangian  
170 multiplier method with displacement  $\mathbf{v}$  regarded as multiplier. Thus, then the  
171 new complementary energy functional namely  $\Pi$  is given by:

$$\begin{aligned}
& \Pi(\mathbf{v}, \varepsilon_{\alpha\beta}, \kappa_{\alpha\beta}, N^{\alpha\beta}, M^{\alpha\beta}) \\
&= \Pi_C(\varepsilon_{\alpha\beta}, \kappa_{\alpha\beta}, N^{\alpha\beta}, M^{\alpha\beta}) + \int_{\Gamma_M} \theta_{\mathbf{n}} (M_{\mathbf{nn}} - \bar{M}_{\mathbf{nn}}) d\Gamma \\
&- \int_{\Gamma_T} \mathbf{v} \cdot (\mathbf{T} - \bar{\mathbf{T}}) d\Gamma - \mathbf{v} \cdot \mathbf{a}_3 (P - \bar{P})_{\mathbf{x} \in C_P} - \int_{\Omega} \mathbf{v} \cdot (\mathbf{b} - \bar{\mathbf{b}}) d\Omega
\end{aligned} \tag{18}$$

where  $\bar{\mathbf{T}}$ ,  $\bar{M}_{nn}$  and  $\bar{P}$  are the prescribed traction, bending moment and concentrated force on edges  $\Gamma_T$ ,  $\Gamma_M$  and corner  $C_P$  respectively. All the boundaries meet the following geometric relationships:

$$\begin{cases} \Gamma = \Gamma_v \cup \Gamma_T \cup \Gamma_\theta \cup \Gamma_M, & C = C_v \cup C_P, \\ \Gamma_v \cap \Gamma_T = \Gamma_\theta \cap \Gamma_M = C_v \cap C_P = \emptyset \end{cases} \quad (19)$$

and  $\bar{\mathbf{b}}$  stands for the prescribed body force in  $\Omega$ ,  $\mathbf{b}$  also can be written based on Euler-Lagrange equations [30] as:

$$\mathbf{b} = \mathbf{b}_N + \mathbf{b}_M \rightarrow \begin{cases} \mathbf{b}_N = (\mathbf{a}_\alpha N^{\alpha\beta})|_\beta \\ \mathbf{b}_M = (\mathbf{a}_3 M^{\alpha\beta})|_{\alpha\beta} \end{cases} \quad (20)$$

Introducing a standard variational argument to Eq. (18),  $\delta\Pi = 0$ , and considering the arbitrariness of virtual variables,  $\delta\mathbf{v}$ ,  $\delta\varepsilon_{\alpha\beta}$ ,  $\delta\kappa_{\alpha\beta}$ ,  $N^{\alpha\beta}$ ,  $M^{\alpha\beta}$  lead to the following weak form:

$$-\int_{\Omega} h\delta\varepsilon_{\alpha\beta} C^{\alpha\beta\gamma\eta} \varepsilon_{\gamma\eta} d\Omega + \int_{\Omega} \delta\varepsilon_{\alpha\beta} N^{\alpha\beta} d\Omega = 0 \quad (21a)$$

$$-\int_{\Omega} \frac{h^3}{12} \delta\kappa_{\alpha\beta} C^{\alpha\beta\gamma\eta} \kappa_{\gamma\eta} d\Omega + \int_{\Omega} \delta\kappa_{\alpha\beta} M^{\alpha\beta} d\Omega = 0 \quad (21b)$$

$$\begin{aligned} \int_{\Omega} \delta N^{\alpha\beta} \varepsilon_{\alpha\beta} d\Omega - \int_{\Gamma} \delta \mathbf{T}_N \cdot \mathbf{v} d\Gamma + \int_{\Omega} \delta \mathbf{b}_N \cdot \mathbf{v} d\Omega \\ + \int_{\Gamma_v} \delta \mathbf{T}_N \cdot \mathbf{v} d\Gamma = \int_{\Gamma_v} \delta \mathbf{T}_N \cdot \bar{\mathbf{v}} d\Gamma \end{aligned} \quad (21c)$$

$$\begin{aligned} \int_{\Omega} \delta M^{\alpha\beta} \kappa_{\alpha\beta} d\Omega - \int_{\Gamma} \delta M_{nn} \theta_n d\Gamma + \int_{\Gamma} \delta \mathbf{T}_M \cdot \mathbf{v} d\Gamma + (\delta P \mathbf{a}_3 \cdot \mathbf{v})_{\mathbf{x} \in C} + \int_{\Omega} \delta \mathbf{b}_M \cdot \mathbf{v} d\Omega \\ + \int_{\Gamma_\theta} \delta M_{nn} \theta_n d\Gamma - \int_{\Gamma_v} \delta \mathbf{T}_M \cdot \mathbf{v} d\Gamma - (\delta P \mathbf{a}_3 \cdot \mathbf{v})_{\mathbf{x} \in C_v} \\ = \int_{\Gamma_\theta} \delta M_{nn} \bar{\theta}_n d\Gamma - \int_{\Gamma_v} \delta \mathbf{T}_M \cdot \bar{\mathbf{v}} d\Gamma - (\delta P \mathbf{a}_3 \cdot \bar{\mathbf{v}})_{\mathbf{x} \in C_v} \end{aligned} \quad (21d)$$

$$\begin{aligned} \int_{\Gamma} \delta \theta_n M_{nn} d\Gamma - \int_{\Gamma} \delta \mathbf{v} \cdot \mathbf{T} d\Gamma - (\delta \mathbf{v} \cdot \mathbf{a}_3 P)_{\mathbf{x} \in C} + \int_{\Omega} \delta \mathbf{v} \cdot \mathbf{b} d\Omega \\ - \int_{\Gamma_\theta} \delta \theta_n M_{nn} d\Gamma + \int_{\Gamma_v} \delta \mathbf{v} \cdot \mathbf{T} d\Gamma + (\delta \mathbf{v} \cdot \mathbf{a}_3 P)_{\mathbf{x} \in C_v} = - \int_{\Gamma_T} \delta \mathbf{v} \cdot \bar{\mathbf{t}} d\Gamma - \int_{\Omega} \delta \mathbf{v} \cdot \bar{\mathbf{b}} d\Omega \end{aligned} \quad (21e)$$

where the geometric relationships of Eq. (19) is used herein.



### 185 3. Mixed meshfree formulation for modified Hellinger-Reissner weak 186 form

#### 187 3.1. Reproducing kernel approximation for displacement

188 This study approximates the displacement by adopting reproducing kernel  
189 approximation. As shown in Fig. 2, the mid-surface of the shell  $\Omega$  is discretized  
190 by a set of meshfree nodes  $\{\boldsymbol{\xi}_I\}_{I=1}^{n_p}$  in parametric configuration, where  $n_p$  is the  
191 total number of meshfree nodes. The approximated displacement namely  $\boldsymbol{v}^h$   
192 can be expressed as:

$$\boldsymbol{v}(\boldsymbol{\xi}) = \sum_{I=1}^{n_p} \Psi_I(\boldsymbol{\xi}) \boldsymbol{d}_I \quad (22)$$

193 in which  $\Psi_I$  and  $\boldsymbol{d}_I$  is the shape function and nodal coefficient tensor related by  
194 node  $\boldsymbol{\xi}_I$ . According to reproducing kernel approximation [4], the shape function  
195 takes the following form:

$$\Psi_I(\boldsymbol{\xi}) = \boldsymbol{p}^T(\boldsymbol{\xi}) \boldsymbol{c}(\boldsymbol{\xi}) \phi(\boldsymbol{\xi}_I - \boldsymbol{\xi}) \quad (23)$$

196 where  $\boldsymbol{p}$  is the basis function vector represented using the following quadratic  
197 function as:

$$\boldsymbol{p} = \{1, \xi^1, \xi^2, (\xi^1)^2, \xi^1 \xi^2, (\xi^2)^2\}^T \quad (24)$$

198 The kernel function denoted by  $\phi$  controls the support and smoothness of  
199 meshfree shape functions. The quintic B-spline function with square support is  
200 used herein as the kernel function:

$$\phi(\boldsymbol{\xi}_I - \boldsymbol{\xi}) = \phi(\hat{s}_1) \phi(\hat{s}_2), \quad \hat{s}_\alpha = \frac{|\xi_I^\alpha - \xi^\alpha|}{s_{\alpha I}} \quad (25)$$

201 with

$$\phi(\hat{s}_\alpha) = \frac{1}{5!} \begin{cases} (3 - 3\hat{s}_\alpha)^5 - 6(2 - 3\hat{s}_\alpha)^5 + 15(1 - 3\hat{s}_\alpha)^5 & \hat{s}_\alpha \leq \frac{1}{3} \\ (3 - 3\hat{s}_\alpha)^5 - 6(2 - 3\hat{s}_\alpha)^5 & \frac{1}{3} < \hat{s}_\alpha \leq \frac{2}{3} \\ (3 - 3\hat{s}_\alpha)^5 & \frac{2}{3} < \hat{s}_\alpha \leq 1 \\ 0 & \hat{s}_\alpha > 1 \end{cases} \quad (26)$$

202 and  $\hat{s}_{\alpha I}$  means the characterized size of support for meshfree shape function  $\Psi_I$ .

203 The unknown vector  $\boldsymbol{c}$  in shape function are determined by the fulfillment  
204 of the so-called consistency condition:

$$\sum_{I=1}^{n_p} \Psi_I(\boldsymbol{\xi}) \boldsymbol{p}(\boldsymbol{\xi}_I) = \boldsymbol{p}(\boldsymbol{\xi}) \quad (27)$$

205 or equivalently

$$\sum_{I=1}^{n_p} \Psi_I(\boldsymbol{\xi}) \boldsymbol{p}(\boldsymbol{\xi}_I - \boldsymbol{\xi}) = \boldsymbol{p}(\mathbf{0}) \quad (28)$$

206 Substituting Eq. (22) into (28), yields:

$$\mathbf{A}(\boldsymbol{\xi})\mathbf{c}(\boldsymbol{\xi}) = \mathbf{p}(\mathbf{0}) \quad \Rightarrow \quad \mathbf{c}(\boldsymbol{\xi}) = \mathbf{A}^{-1}(\boldsymbol{\xi})\mathbf{p}(\mathbf{0}) \quad (29)$$

207 where  $\mathbf{A}$  is the moment matrix:

$$\mathbf{A}(\boldsymbol{\xi}) = \sum_{I=1}^{n_p} \phi(\boldsymbol{\xi}_I - \boldsymbol{\xi}) \mathbf{p}(\boldsymbol{\xi}_I - \boldsymbol{\xi}) \mathbf{p}^T(\boldsymbol{\xi}_I - \boldsymbol{\xi}) \quad (30)$$

208 Substituting Eq. (29) back into Eq. (22), the expression of meshfree shape  
209 function can be written as:

$$\Psi_I(\boldsymbol{\xi}) = \mathbf{p}^T(\boldsymbol{\xi}_I - \boldsymbol{\xi}) \mathbf{A}^{-1}(\boldsymbol{\xi}) \mathbf{p}(\mathbf{0}) \phi(\boldsymbol{\xi}_I - \boldsymbol{\xi}) \quad (31)$$

### 210 3.2. Reproducing kernel gradient smoothing approximation for effective stress 211 and strain

212 In Galerkin meshfree formulation, the mid-plane of thin shell  $\Omega$  is split by  
213 a set of integration cells  $\Omega_C$ 's,  $\cup_{C=1}^{n_e} \Omega_C \approx \Omega$ , as shown in Fig. 2. With the  
214 inspiration of reproducing kernel smoothing framework, the Cartesian and co-  
215 variant derivatives of displacement,  $\mathbf{v}_{,\alpha}$  and  $-\mathbf{v}_{,\alpha}|_{\beta}$ , in strains  $\varepsilon_{\alpha\beta}$ ,  $\kappa_{\alpha\beta}$  are  
216 approximated by  $(p-1)$ -th order polynomials in each integration cells. In inte-  
217 gration cell  $\Omega_C$ , the approximated derivatives and strains denoted by  $\mathbf{v}_{,\alpha}^h$ ,  $\varepsilon_{\alpha\beta}^h$   
218 and  $-\mathbf{v}_{,\alpha}^h|_{\beta}$ ,  $\kappa_{\alpha\beta}^h$  can be expressed by:

$$\mathbf{v}_{,\alpha}^h(\boldsymbol{\xi}) = \mathbf{q}^T(\boldsymbol{\xi}) \mathbf{d}_{\alpha}^{\varepsilon}, \quad \varepsilon_{\alpha\beta}^h(\boldsymbol{\xi}) = \mathbf{q}^T(\boldsymbol{\xi}) \frac{1}{2} (\mathbf{a}_{\alpha} \cdot \mathbf{d}_{\beta}^{\varepsilon} + \mathbf{a}_{\beta} \cdot \mathbf{d}_{\alpha}^{\varepsilon}) \quad (32)$$

$$-\mathbf{v}_{,\alpha}^h|_{\beta}(\boldsymbol{\xi}) = \mathbf{q}^T(\boldsymbol{\xi}) \mathbf{d}_{\alpha\beta}^{\kappa}, \quad \kappa_{\alpha\beta}^h(\boldsymbol{\xi}) = \mathbf{q}^T(\boldsymbol{\xi}) \mathbf{a}_3 \cdot \mathbf{d}_{\alpha\beta}^{\kappa} \quad (33)$$

220 where  $\mathbf{q}$  is the linear polynomial vector and has the following form:

$$\mathbf{q} = \{1, \xi^1, \xi^2\}^T \quad (34)$$

221 and the  $\mathbf{d}_{\alpha}^{\varepsilon}$ ,  $\mathbf{d}_{\alpha\beta}^{\kappa}$  are the corresponding coefficient vector tensors. For the con-  
222 ciseness, the mixed usage of tensor and vector is introduced in this study. For  
223 instance, the component of coefficient tensor vector  $\mathbf{d}_{\alpha I}^{\varepsilon}$ ,  $\mathbf{d}_{\alpha}^{\varepsilon} = \{\mathbf{d}_{\alpha I}^{\varepsilon}\}$ , is a three  
224 dimensional tensor,  $\dim \mathbf{d}_{\alpha I}^{\varepsilon} = \dim \mathbf{v}$ .

225 In order to meet the integration constraint of thin shell problem, the ap-  
226 proximated stresses  $N^{\alpha\beta h}$ ,  $M^{\alpha\beta h}$  are assumed to be a similar form with strains,  
227 yields:

$$N^{\alpha\beta h}(\boldsymbol{\xi}) = \mathbf{q}^T(\boldsymbol{\xi}) \mathbf{a}^{\alpha} \cdot \mathbf{d}_N^{\beta}, \quad \mathbf{a}_{\alpha} N^{\alpha\beta h}(\boldsymbol{\xi}) = \mathbf{q}^T(\boldsymbol{\xi}) \mathbf{d}_N^{\beta} \quad (35)$$

$$M^{\alpha\beta h}(\boldsymbol{\xi}) = \mathbf{q}^T(\boldsymbol{\xi}) \mathbf{a}_3 \cdot \mathbf{d}_M^{\alpha\beta}, \quad \mathbf{a}_3 M^{\alpha\beta h}(\boldsymbol{\xi}) = \mathbf{q}^T(\boldsymbol{\xi}) \mathbf{d}_M^{\alpha\beta} \quad (36)$$

229 substituting the approximations of Eqs. (22), (32), (33), (35), (36) into Eqs.  
230 (21c), (21d) can express  $\mathbf{d}_{\beta}^{\varepsilon}$  and  $\mathbf{d}_{\alpha\beta}^{\kappa}$  by  $\mathbf{d}$  as:

$$\mathbf{d}_{\beta}^{\varepsilon} = \mathbf{G}^{-1} \left( \sum_{I=1}^{n_p} (\tilde{\mathbf{g}}_{\beta I} - \bar{\mathbf{g}}_{\beta I}) \mathbf{d}_I + \hat{\mathbf{g}}_{\beta} \right) \quad (37)$$

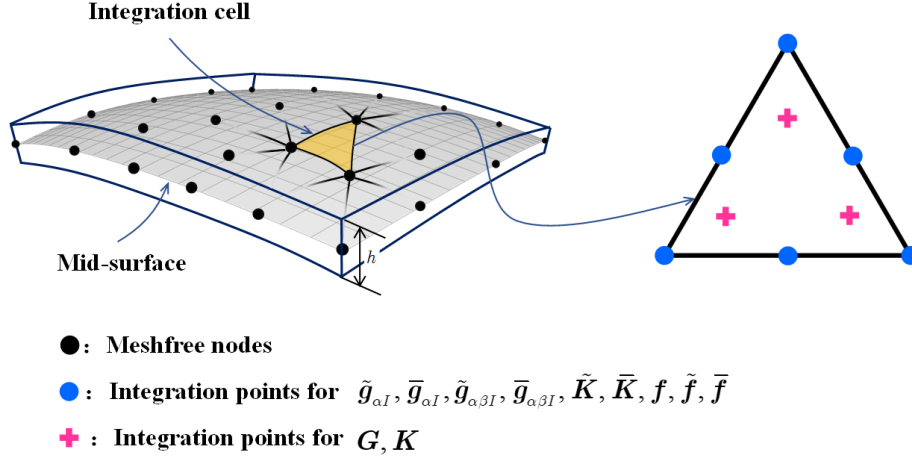


Figure 2: Integration scheme for Hu-Washizu weak form.

231

$$d_{\alpha\beta}^{\kappa} = G^{-1} \left( \sum_{I=1}^{n_p} (\tilde{g}_{\alpha\beta I} - \bar{g}_{\alpha\beta I}) d_I + \hat{g}_{\alpha\beta} \right) \quad (38)$$

232 with

$$G = \int_{\Omega_C} q^T q d\Omega \quad (39)$$

233

$$\tilde{g}_{\beta I} = \int_{\Gamma_C} \Psi_I q n_{\beta} d\Gamma - \int_{\Omega_C} \Psi_I q_{|\beta} d\Omega \quad (40a)$$

$$\bar{g}_{\beta I} = \int_{\Gamma_C \cap \Gamma_v} \Psi_I q n_{\beta} d\Gamma \quad (40b)$$

$$\hat{g}_{\beta} = \int_{\Gamma_C \cap \Gamma_v} q n_{\beta} \bar{v} d\Gamma \quad (40c)$$

234

$$\begin{aligned} \tilde{g}_{\alpha\beta I} = & \int_{\Gamma_C} \Psi_{I,\gamma} n^{\gamma} q n_{\alpha} n_{\beta} d\Gamma - \int_{\Gamma_C} \Psi_I (q_{|\beta} n_{\alpha} + (q s_{\alpha} n_{\beta})_{,\gamma} s^{\gamma}) d\Gamma \\ & + [[\Psi_I q s_{\alpha} n_{\beta}]]_{\mathbf{x} \in C_C} - \int_{\Omega_C} \Psi q_{,\alpha|\beta} d\Omega \end{aligned} \quad (41a)$$

$$\begin{aligned} \bar{g}_{\alpha\beta I} = & \int_{\Gamma_C \cap \Gamma_{\theta}} \Psi_{I,\gamma} n^{\gamma} q n_{\alpha} n_{\beta} d\Gamma - \int_{\Gamma_C \cap \Gamma_v} \Psi_I (q_{|\beta} n_{\alpha} + (q s_{\alpha} n_{\beta})_{,\gamma} s^{\gamma}) d\Gamma \\ & + [[\Psi_I q s_{\alpha} n_{\beta}]]_{\mathbf{x} \in C_C \cap C_v} \end{aligned} \quad (41b)$$

$$\begin{aligned} \hat{g}_{\alpha\beta} = & \int_{\Gamma_C \cap \Gamma_{\theta}} q n_{\alpha} n_{\beta} a_3 \bar{\theta}_{\mathbf{n}} d\Gamma - \int_{\Gamma_C \cap \Gamma_v} (q_{|\beta} n_{\alpha} + (q s_{\alpha} n_{\beta})_{,\gamma} s^{\gamma}) \bar{v} d\Gamma \\ & + [[q s_{\alpha} n_{\beta} \bar{v}]]_{\mathbf{x} \in C_C \cap C_v} \end{aligned} \quad (41c)$$

where evaluations of  $\mathbf{q}_{|\beta}$ ,  $\mathbf{q}_{,\alpha|\beta}$  are detail in Appendix A. Further plugging Eqs. (37) and (38) back into Eqs. (32) and (33) respectively gives the final expression of  $\mathbf{v}_{,\alpha}^h$ ,  $\varepsilon_{\alpha\beta}^h$  and  $-\mathbf{v}_{,\alpha\beta}^h$ ,  $\kappa_{\alpha\beta}^h$  as:

$$\mathbf{v}_{,\alpha}^h = \sum_{I=1}^{n_p} (\tilde{\Psi}_{I,\alpha} - \bar{\Psi}_{I,\alpha}) \mathbf{d}_I + \mathbf{q}^T \mathbf{G}^{-1} \hat{\mathbf{g}}_\alpha \quad (42a)$$

$$\begin{aligned} \varepsilon_{\alpha\beta}^h &= \sum_{I=1}^{n_p} \frac{1}{2} (\mathbf{a}_\alpha \tilde{\Psi}_{I,\beta} + \mathbf{a}_\beta \tilde{\Psi}_{I,\alpha}) \cdot \mathbf{d}_I - \sum_{I=1}^{n_p} \frac{1}{2} (\mathbf{a}_\alpha \bar{\Psi}_{I,\beta} + \mathbf{a}_\beta \bar{\Psi}_{I,\alpha}) \cdot \mathbf{d}_I \\ &\quad + \mathbf{q}^T \mathbf{G}^{-1} \frac{1}{2} (\mathbf{a}_\alpha \cdot \hat{\mathbf{g}}_\beta + \mathbf{a}_\beta \cdot \hat{\mathbf{g}}_\alpha) \\ &= \tilde{\varepsilon}_{\alpha\beta}^h - \bar{\varepsilon}_{\alpha\beta}^h + \hat{\varepsilon}_{\alpha\beta}^h \end{aligned} \quad (42b)$$

$$-\mathbf{v}_{,\alpha\beta}^h = \sum_{I=1}^{n_p} (\tilde{\Psi}_{I,\alpha\beta} - \bar{\Psi}_{I,\alpha\beta}) \mathbf{d}_I + \mathbf{q}^T \mathbf{G}^{-1} \hat{\mathbf{g}}_{\alpha\beta} \quad (43a)$$

$$\begin{aligned} \kappa_{\alpha\beta}^h &= \sum_{I=1}^{n_p} \tilde{\Psi}_{I,\alpha\beta} \mathbf{a}_3 \cdot \mathbf{d}_I - \sum_{I=1}^{n_p} \bar{\Psi}_{I,\alpha\beta} \mathbf{a}_3 \cdot \mathbf{d}_I + \mathbf{q}^T \mathbf{G}^{-1} \mathbf{a}_3 \cdot \hat{\mathbf{g}}_{\alpha\beta} \\ &= \tilde{\kappa}_{\alpha\beta}^h - \bar{\kappa}_{\alpha\beta}^h + \hat{\kappa}_{\alpha\beta}^h \end{aligned} \quad (43b)$$

with

$$\begin{cases} \tilde{\varepsilon}_{\alpha\beta}^h = \sum_{I=1}^{n_p} \frac{1}{2} (\mathbf{a}_\alpha \tilde{\Psi}_{I,\beta} + \mathbf{a}_\beta \tilde{\Psi}_{I,\alpha}) \cdot \mathbf{d}_I = \sum_{I=1}^{n_p} \tilde{\varepsilon}_{\alpha\beta I} \cdot \mathbf{d}_I \\ \bar{\varepsilon}_{\alpha\beta}^h = \sum_{I=1}^{n_p} \frac{1}{2} (\mathbf{a}_\alpha \bar{\Psi}_{I,\beta} + \mathbf{a}_\beta \bar{\Psi}_{I,\alpha}) \cdot \mathbf{d}_I = \sum_{I=1}^{n_p} \bar{\varepsilon}_{\alpha\beta I} \cdot \mathbf{d}_I \\ \hat{\varepsilon}_{\alpha\beta}^h = \mathbf{q}^T \mathbf{G}^{-1} \frac{1}{2} (\mathbf{a}_\alpha \cdot \hat{\mathbf{g}}_\beta + \mathbf{a}_\beta \cdot \hat{\mathbf{g}}_\alpha) \end{cases} \quad (44)$$

$$\begin{cases} \tilde{\Psi}_{I,\alpha}(\boldsymbol{\xi}) = \mathbf{q}^T(\boldsymbol{\xi}) \mathbf{G}^{-1} \tilde{\mathbf{g}}_{\alpha I} \\ \bar{\Psi}_{I,\alpha}(\boldsymbol{\xi}) = \mathbf{q}^T(\boldsymbol{\xi}) \mathbf{G}^{-1} \bar{\mathbf{g}}_{\alpha I} \\ \tilde{\varepsilon}_{\alpha\beta I} = \frac{1}{2} (\mathbf{a}_\alpha \tilde{\Psi}_{I,\beta} + \mathbf{a}_\beta \tilde{\Psi}_{I,\alpha}) \\ \bar{\varepsilon}_{\alpha\beta I} = \frac{1}{2} (\mathbf{a}_\alpha \bar{\Psi}_{I,\beta} + \mathbf{a}_\beta \bar{\Psi}_{I,\alpha}) \end{cases} \quad (45)$$

$$\begin{cases} \tilde{\kappa}_{\alpha\beta}^h = \sum_{I=1}^{n_p} \tilde{\Psi}_{I,\alpha\beta} \mathbf{a}_3 \cdot \mathbf{d}_I = \sum_{I=1}^{n_p} \tilde{\kappa}_{\alpha\beta I} \cdot \mathbf{d}_I \\ \bar{\kappa}_{\alpha\beta}^h = \sum_{I=1}^{n_p} \bar{\Psi}_{I,\alpha\beta} \mathbf{a}_3 \cdot \mathbf{d}_I = \sum_{I=1}^{n_p} \bar{\kappa}_{\alpha\beta I} \cdot \mathbf{d}_I \\ \hat{\kappa}_{\alpha\beta}^h = \mathbf{q}^T \mathbf{G}^{-1} \mathbf{a}_3 \cdot \hat{\mathbf{g}}_{\alpha\beta} \end{cases} \quad (46)$$

$$\begin{cases} \tilde{\Psi}_{I,\alpha\beta}(\boldsymbol{\xi}) = \mathbf{q}^T(\boldsymbol{\xi})\mathbf{G}^{-1}\tilde{\mathbf{g}}_{\alpha\beta I} \\ \bar{\Psi}_{I,\alpha\beta}(\boldsymbol{\xi}) = \mathbf{q}^T(\boldsymbol{\xi})\mathbf{G}^{-1}\tilde{\mathbf{g}}_{\alpha\beta I} \\ \tilde{\boldsymbol{\kappa}}_{\alpha\beta I} = \tilde{\Psi}_{I,\alpha\beta}\mathbf{a}_3 \\ \bar{\boldsymbol{\kappa}}_{\alpha\beta I} = \bar{\Psi}_{I,\alpha\beta}\mathbf{a}_3 \end{cases} \quad (47)$$

245 It has to be noted that, referring to reproducing kernel gradient smoothing  
 246 framework [25],  $\tilde{\Psi}_{I,\alpha}$ ,  $\tilde{\Psi}_{I,\alpha\beta}$  are actually the first and second order smoothed  
 247 gradients in curvilinear coordinates.  $\tilde{\mathbf{g}}_{\alpha I}$  and  $\tilde{\mathbf{g}}_{\alpha\beta I}$  are the right hand side in-  
 248 tegration constraints for first and second order gradients, then this formulation  
 249 can meet the variational consistency for the  $p$ -th order polynomials. It should  
 250 be known that, in curved model, the variational consistency for non-polynomial  
 251 functions, like trigonometric functions, should be required for the polynomial  
 252 solution. Even with  $p$ -th order variational consistency, the proposed formulation  
 253 can not exactly reproduce the solution spanned by basis functions. However,  
 254 the accuracy of reproducing kernel smoothed gradients is still better than tradi-  
 255 tional meshfree formulation. Numerical examples in the section below will pro-  
 256 vide better evidence to prove the accuracy of the reproducing kernel smoothed  
 257 gradients.

258 **4. Naturally variational enforcement for essential boundary condi-**  
 259 **tions**

260 *4.1. Discrete equilibrium equations*

261 With the approximated effective stresses and strains, the last equation of  
 262 weak form Eq. (21e) becomes:

$$-\sum_{C=1}^{n_e} \sum_{I=1}^{n_p} \delta \mathbf{d}_I \cdot \left( (\tilde{\mathbf{g}}_{\alpha I}^T - \bar{\mathbf{g}}_{\alpha I}^T) \mathbf{d}_N^\alpha + (\tilde{\mathbf{g}}_{\alpha \beta I}^T - \bar{\mathbf{g}}_{\alpha \beta I}^T) \mathbf{d}_M^{\alpha \beta} \right) = -\sum_{I=1}^{n_p} \delta \mathbf{d}_I \cdot \mathbf{f}_I \quad (48)$$

263 where  $\mathbf{f}_I$ 's are the components of the traditional force vector:

$$\mathbf{f}_I = \int_{\Gamma_t} \Psi_I \bar{\mathbf{t}} d\Gamma - \int_{\Gamma_M} \Psi_{I,\gamma} n^\gamma \bar{M}_{nn} d\Gamma + [[\Psi_I \mathbf{a}_3 \bar{P}]]_{\mathbf{x} \in C_P} + \int_{\Omega} \Psi_I \bar{\mathbf{b}} d\Omega \quad (49)$$

264 The left side of Eq. (48) can be simplified using the following steps. For clarity,  
 265 the derivation of first term in Eq. (48) taken as an example is given by:

$$\begin{aligned} \sum_{I=1}^{n_p} \delta \mathbf{d}_I \cdot \tilde{\mathbf{g}}_{\alpha I}^T \mathbf{d}_N^\alpha &= \sum_{I=1}^{n_p} \delta \mathbf{d}_I \cdot (\mathbf{G}^{-1} \tilde{\mathbf{g}}_{\alpha I})^T \mathbf{G} \mathbf{d}_N^\alpha \\ &= \int_{\Omega_C} \sum_{I=1}^{n_p} \delta \mathbf{d}_I \cdot (\mathbf{q}^T \mathbf{G}^{-1} \tilde{\mathbf{g}}_{\alpha I})^T \mathbf{q}^T \mathbf{d}_N^\alpha d\Omega \\ &= \int_{\Omega_C} \sum_{I=1}^{n_p} \delta \mathbf{d}_I \cdot \mathbf{a}_\beta (\mathbf{q}^T \mathbf{G}^{-1} \tilde{\mathbf{g}}_{\alpha I})^T N^{\alpha \beta h} d\Omega \\ &= \int_{\Omega_C} \delta \tilde{\varepsilon}_{\alpha \beta}^h N^{\alpha \beta h} d\Omega \end{aligned} \quad (50)$$

266 following the above procedure and including the weak form of Eqs. (21a), (21b),  
 267 the left side of Eq. (48) in  $\Omega_C$  becomes:

$$\begin{aligned}
 & \sum_{I=1}^{n_p} \delta \mathbf{d}_I \cdot \left( (\tilde{\mathbf{g}}_{\alpha I}^T - \bar{\mathbf{g}}_{\alpha I}^T) \mathbf{d}_N^\alpha + (\tilde{\mathbf{g}}_{\alpha \beta I}^T - \bar{\mathbf{g}}_{\alpha \beta I}^T) \mathbf{d}_M^{\alpha \beta} \right) \\
 &= \int_{\Omega_C} ((\delta \tilde{\varepsilon}_{\alpha \beta}^h - \delta \bar{\varepsilon}_{\alpha \beta}^h) N^{\alpha \beta h} + (\delta \tilde{\kappa}_{\alpha \beta}^h - \delta \bar{\kappa}_{\alpha \beta}^h) M^{\alpha \beta h}) d\Omega \\
 &= \int_{\Omega_C} (\delta \tilde{\varepsilon}_{\alpha \beta}^h - \delta \bar{\varepsilon}_{\alpha \beta}^h) h C^{\alpha \beta \gamma \eta} \varepsilon_{\gamma \eta}^h + (\delta \tilde{\kappa}_{\alpha \beta}^h - \delta \bar{\kappa}_{\alpha \beta}^h) \frac{h^3}{12} C^{\alpha \beta \gamma \eta} \kappa_{\gamma \eta}^h \\
 &= \int_{\Omega_C} \delta \tilde{\varepsilon}_{\alpha \beta}^h h C^{\alpha \beta \gamma \eta} \varepsilon_{\gamma \eta}^h d\Omega + \int_{\Omega_C} \delta \tilde{\kappa}_{\alpha \beta}^h \frac{h^3}{12} C^{\alpha \beta \gamma \eta} \kappa_{\gamma \eta}^h d\Omega \\
 &\quad - \int_{\Omega_C} \delta \bar{\varepsilon}_{\alpha \beta}^h h C^{\alpha \beta \gamma \eta} \varepsilon_{\gamma \eta}^h d\Omega - \int_{\Omega_C} \delta \bar{\kappa}_{\alpha \beta}^h h C^{\alpha \beta \gamma \eta} \kappa_{\gamma \eta}^h d\Omega \\
 &\quad - \int_{\Omega_C} \delta \tilde{\kappa}_{\alpha \beta}^h \frac{h^3}{12} C^{\alpha \beta \gamma \eta} \bar{\kappa}_{\gamma \eta}^h d\Omega - \int_{\Omega_C} \delta \bar{\kappa}_{\alpha \beta}^h \frac{h^3}{12} C^{\alpha \beta \gamma \eta} \tilde{\kappa}_{\gamma \eta}^h d\Omega \\
 &\quad + \int_{\Omega_C} \delta \bar{\varepsilon}_{\alpha \beta}^h h C^{\alpha \beta \gamma \eta} \varepsilon_{\gamma \eta}^h d\Omega + \int_{\Omega_C} \delta \bar{\kappa}_{\alpha \beta}^h \frac{h^3}{12} C^{\alpha \beta \gamma \eta} \bar{\kappa}_{\gamma \eta}^h d\Omega \\
 &\quad + \int_{\Omega_C} (\delta \tilde{\varepsilon}_{\alpha \beta}^h - \delta \bar{\varepsilon}_{\alpha \beta}^h) h C^{\alpha \beta \gamma \eta} \varepsilon_{\gamma \eta}^h d\Omega + \int_{\Omega_C} (\delta \tilde{\kappa}_{\alpha \beta}^h - \delta \bar{\kappa}_{\alpha \beta}^h) \frac{h^3}{12} C^{\alpha \beta \gamma \eta} \hat{\kappa}_{\gamma \eta}^h d\Omega
 \end{aligned} \tag{51}$$

268 on further substituting Eqs. (44) and (46) into above equation gives the final  
 269 discrete equilibrium equations, respectively:

$$(\mathbf{K} + \tilde{\mathbf{K}} + \bar{\mathbf{K}}) \mathbf{d} = \mathbf{f} + \tilde{\mathbf{f}} + \bar{\mathbf{f}} \tag{52}$$

270 where

$$\mathbf{K}_{IJ} = \int_{\Omega} \tilde{\varepsilon}_{\alpha \beta I} h C^{\alpha \beta \gamma \eta} \tilde{\varepsilon}_{\gamma \eta J} d\Omega + \int_{\Omega} \tilde{\kappa}_{\alpha \beta I} \frac{h^3}{12} C^{\alpha \beta \gamma \eta} \tilde{\kappa}_{\alpha \beta J} d\Omega \tag{53}$$

271

$$\begin{aligned}
 \tilde{\mathbf{K}}_{IJ} &= - \int_{\Gamma_v} (\Psi_I \tilde{\mathbf{T}}_{NJ} + \tilde{\mathbf{T}}_{NJ} \Psi_J) d\Gamma \\
 &\quad + \int_{\Gamma_\theta} (\Psi_{I,\gamma} n^\gamma \mathbf{a}_3 \tilde{\mathbf{M}}_{nnJ} + \mathbf{a}_3 \tilde{\mathbf{M}}_{nnI} \Psi_{J,\gamma} n^\gamma) d\Gamma
 \end{aligned} \tag{54a}$$

$$\begin{aligned}
 &\quad + ([[\Psi_I \mathbf{a}_3 \tilde{\mathbf{P}}_J]] + [[\tilde{\mathbf{P}}_I \mathbf{a}_3 \Psi_J]])_{\mathbf{x} \in C_v} \\
 \tilde{\mathbf{f}}_I &= - \int_{\Gamma_v} \tilde{\mathbf{T}}_{NI} \cdot \bar{\mathbf{v}} d\Gamma + \int_{\Gamma_\theta} \tilde{\mathbf{M}}_{nnI} \bar{\theta}_n d\Gamma + [[\tilde{\mathbf{P}}_I \mathbf{a}_3 \cdot \bar{\mathbf{v}}]]_{\mathbf{x} \in C_v}
 \end{aligned} \tag{54b}$$

272

$$\bar{\mathbf{K}}_{IJ} = - \int_{\Gamma_v} \bar{\mathbf{T}}_{MI} \Psi_J d\Gamma + \int_{\Gamma_\theta} \mathbf{a}_3 \bar{\mathbf{M}}_{nnI} \Psi_{J,\gamma} n^\gamma d\Gamma + [[\bar{\mathbf{P}}_I \mathbf{a}_3 \Psi_J]]_{\mathbf{x} \in C_v} \tag{55a}$$

$$\bar{\mathbf{f}}_I = - \int_{\Gamma_v} \bar{\mathbf{T}}_{MI} \cdot \bar{\mathbf{v}} d\Gamma + \int_{\Gamma_\theta} \bar{\mathbf{M}}_{nnI} \bar{\theta}_n d\Gamma + [[\bar{\mathbf{P}}_I \mathbf{a}_3 \cdot \bar{\mathbf{v}}]]_{\mathbf{x} \in C_v} \tag{55b}$$

273 The detailed derivations of Eqs (53)-(55) are listed in the Appendix B. As  
 274 shown in these equations, Eq. (53) is the conventional stiffness matrix evaluated  
 275 by smoothed gradients  $\tilde{\Psi}_{I,\alpha}$ ,  $\tilde{\Psi}_{I,\alpha}|_\beta$ , and the Eqs. (54) and (55) contribute for  
 276 the enforcement of essential boundary. It should be mentioned that, in accor-  
 277 dance with reproducing kernel smoothed gradient framework, the integration  
 278 scheme of Eqs. (53-55) should be aligned with the those used in the construc-  
 279 tion of smoothed gradients. The integration scheme used for proposed method  
 280 is shown in Fig. 2, the detailed positions and weight of integration points can  
 281 be found in [31] With a close look at Eqs. (54) and (55), the proposed approach  
 282 for enforcing essential boundary conditions show an identical structure with tra-  
 283 ditional Nitsche's method, both have the consistent and stabilized terms. So,  
 284 the next subsection will review the Nitsche's method and compare it with the  
 285 proposed method.

#### 286 4.2. Comparison with Nitsche's method

287 The Nitsche's method for enforcing essential boundaries can be regarded as a  
 288 combination of Lagrangian multiplier method and penalty method, in which the  
 289 Lagrangian multiplier is represented by the approximated displacement. The  
 290 corresponding total potential energy functional  $\Pi_P$  is given by:

$$\begin{aligned}
 \Pi_P(\mathbf{v}) = & \int_{\Omega} \frac{1}{2} \varepsilon_{\alpha\beta} N^{\alpha\beta} d\Omega + \int_{\Omega} \frac{1}{2} \kappa_{\alpha\beta} M^{\alpha\beta} d\Omega \\
 & - \int_{\Gamma_t} \mathbf{v} \cdot \bar{\mathbf{t}} d\Gamma + \int_{\Gamma_M} \mathbf{v}_{,\gamma} n^\gamma \mathbf{a}_3 M_{\mathbf{n}\mathbf{n}} d\Gamma + (\mathbf{v} \cdot \mathbf{a}_3 P)_{\mathbf{x} \in C_P} - \int_{\Omega} \mathbf{v} \cdot \bar{\mathbf{b}} d\Omega \\
 & - \underbrace{\int_{\Gamma_v} \mathbf{t} \cdot (\mathbf{v} - \bar{\mathbf{v}}) d\Gamma + \int_{\Gamma_\theta} M_{\mathbf{n}\mathbf{n}} (\theta_{\mathbf{n}} - \bar{\theta}_{\mathbf{n}}) d\Gamma + (P \mathbf{a}_3 \cdot (\mathbf{v} - \bar{\mathbf{v}}))_{\mathbf{x} \in C_v}}_{\text{consistent term}} \quad (56) \\
 & + \underbrace{\frac{\alpha_v}{2} \int_{\Gamma_v} \mathbf{v} \cdot \mathbf{v} d\Gamma + \frac{\alpha_\theta}{2} \int_{\Gamma_\theta} \theta_{\mathbf{n}}^2 d\Gamma + \frac{\alpha_C}{2} (\mathbf{v} \cdot \mathbf{v})_{\mathbf{x} \in C_v}}_{\text{stabilized term}}
 \end{aligned}$$

291 where the consistent term generated from the Lagrangian multiplier method  
 292 contributes to enforce the essential boundary, and meet the variational con-  
 293 sistency condition. However, the consistent term can not always ensure the  
 294 coercivity of stiffness, so the penalty method is introduced to serve as a sta-  
 295 bilized term. With a standard variational argument, the corresponding weak



form can be stated as:

$$\begin{aligned}
\delta\Pi_P(\mathbf{v}) &= \int_{\Omega} \delta\varepsilon_{\alpha\beta} N^{\alpha\beta} d\Omega + \int_{\Omega} \delta\kappa_{\alpha\beta} M^{\alpha\beta} d\Omega \\
&\quad - \int_{\Gamma_t} \delta\mathbf{v} \cdot \bar{\mathbf{t}} d\Gamma + \int_{\Gamma_M} \delta\mathbf{v}_{,\gamma} n^{\gamma} \mathbf{a}_3 M_{nn} d\Gamma + (\delta\mathbf{v} \cdot \mathbf{a}_3 P)_{\mathbf{x} \in C_P} - \int_{\Omega} \delta\mathbf{v} \cdot \bar{\mathbf{b}} d\Omega \\
&\quad - \int_{\Gamma_v} \delta\mathbf{v} \cdot \mathbf{t} d\Gamma + \int_{\Gamma_{\theta}} \delta\theta_{\mathbf{n}} M_{nn} d\Gamma + (\mathbf{v} \cdot \mathbf{a}_3 P)_{\mathbf{x} \in C_v} \\
&\quad - \int_{\Gamma_v} \delta\mathbf{t} \cdot (\mathbf{v} - \bar{\mathbf{v}}) d\Gamma + \int_{\Gamma_{\theta}} \delta M_{nn} (\theta_{\mathbf{n}} - \bar{\theta}_{\mathbf{n}}) d\Gamma + (\delta P \mathbf{a}_3 \cdot (\mathbf{v} - \bar{\mathbf{v}}))_{\mathbf{x} \in C_v} \\
&\quad + \alpha_v \int_{\Gamma_v} \delta\mathbf{v} \cdot \mathbf{v} d\Gamma + \alpha_{\theta} \int_{\Gamma_{\theta}} \delta\theta_{\mathbf{n}} \theta_{\mathbf{n}} d\Gamma + \alpha_C (\delta\mathbf{v} \cdot \mathbf{v})_{\mathbf{x} \in C_v} \\
&= 0
\end{aligned} \tag{57}$$

in which  $\alpha_v$ ,  $\alpha_{\theta}$  and  $\alpha_C$  represent experimental artificial parameters. Further invoking the conventional reproducing kernel approximation of Eq. (22) leads to the following discrete equilibrium equations:

$$\sum_{J=1}^{n_p} (\mathbf{K}_{IJ} + \mathbf{K}_{IJ}^c + \mathbf{K}_{IJ}^s) \mathbf{d}_J = \mathbf{f}_I + \mathbf{f}^c + \mathbf{f}^s \tag{58}$$

where the stiffness  $\mathbf{K}_{IJ}$  is identical with Eq. (53).  $\mathbf{K}_{IJ}^c$  and  $\mathbf{K}_{IJ}^s$  are the stiffness matrices for consistent and stabilized terms, respectively, and have the following form:

$$\begin{aligned}
\mathbf{K}_{IJ}^c &= - \int_{\Gamma_v} (\Psi_I \mathbf{T}_{NJ} + \mathbf{T}_{NJ} \Psi_J) d\Gamma \\
&\quad + \int_{\Gamma_{\theta}} (\Psi_{I,\gamma} n^{\gamma} \mathbf{a}_3 \mathbf{M}_{nnJ} + \mathbf{a}_3 \mathbf{M}_{nnI} \Psi_{I,\gamma} n^{\gamma}) d\Gamma \\
&\quad + ([[\Psi_I \mathbf{a}_3 \mathbf{P}_J]] + [[\mathbf{P}_I \mathbf{a}_3 \Psi_J]])_{\mathbf{x} \in C_v}
\end{aligned} \tag{59a}$$

$$\mathbf{f}_I^c = - \int_{\Gamma_v} \mathbf{T}_I \cdot \bar{\mathbf{v}} d\Gamma + \int_{\Gamma_{\theta}} \mathbf{M}_{nnI} \bar{\theta}_{\mathbf{n}} d\Gamma + [[\mathbf{P}_I \mathbf{a}_3 \cdot \bar{\mathbf{v}}]]_{\mathbf{x} \in C_v} \tag{59b}$$

303

$$\mathbf{K}_{IJ}^s = \alpha_v \int_{\Gamma_v} \Psi_I \Psi_J \mathbf{1} d\Gamma + \alpha_{\theta} \int_{\Gamma_{\theta}} \Psi_{I,\eta} n^{\eta} \mathbf{a}_3 \mathbf{a}_3 n^{\gamma} \Psi_{J,\gamma} d\Gamma + \alpha_C [[\Psi_I \mathbf{a}_3 \mathbf{a}_3 \Psi_J]]_{\mathbf{x} \in C_v} \tag{60a}$$

$$\mathbf{f}_I^s = \alpha_v \int_{\Gamma_v} \Psi_I \bar{\mathbf{v}} d\Gamma + \alpha_{\theta} \int_{\Gamma_{\theta}} \Psi_{I,\eta} n^{\eta} \mathbf{a}_3 \bar{\theta}_{\mathbf{n}} d\Gamma + \alpha_C [[\Psi_I \mathbf{a}_3 \mathbf{a}_3 \cdot \bar{\mathbf{v}}]]_{\mathbf{x} \in C_v} \tag{60b}$$

On comparing with the consistent terms of Eqs. (54) and (59), the expressions were almost identical, the major difference is that the higher order derivatives of shape functions have been replaced by smoothed gradients. Owing to

307 the reproducing kernel framework, the construction of smoothed gradients only  
308 concerned about the computation of traditional meshfree shape functions and  
309 their first order derivatives, which avoid the costly computation of higher order  
310 derivatives. Moreover, the stabilized terms in Eq. (60) employs the penalty  
311 method to ensure the coercivity of stiffness. In contrast, the stabilized term of  
312 Eq. (55) naturally exists in its weak form, and can stabilize the result without  
313 considering any artificial parameters.

## 314 5. Numerical examples

315 The suggested method, which uses Nitsche's method, the consistent repro-  
 316 ducing kernel gradient smoothing integration scheme (RKGSI), and the non-  
 317 consistent Gauss integration scheme (GI) with penalty method, as well as the  
 318 proposed Hu-Washizu formulation (HW) to enforce the necessary boundary con-  
 319 ditions, is validated in this section through several examples. A normalized  
 320 support size of 2.5 is used for all the methods to ensure the requirement of  
 321 quadratic base meshfree approximation. To eliminate the influence of integra-  
 322 tion, the Gauss integration scheme uses 6 Gauss points for domain integration  
 323 and 3 points for boundary integration, so as to maintain the same integration  
 324 accuracy between domain and boundaries. Moreover, the number of integra-  
 325 tion points are identical between the Gauss and RKGSI schemes. The error  
 326 estimates of displacement ( $L_2$ -Error) and energy ( $H_e$ -Error) is used here:

$$\begin{aligned}
 L_2\text{-Error} &= \frac{\sqrt{\int_{\Omega} (\mathbf{v} - \mathbf{v}^h) \cdot (\mathbf{v} - \mathbf{v}^h) d\Omega}}{\sqrt{\mathbf{v} \cdot \mathbf{v}}} \\
 H_e\text{-Error} &= \frac{\sqrt{\int_{\Omega} \left( (\varepsilon_{\alpha\beta} - \varepsilon_{\alpha\beta}^h)(N^{\alpha\beta} - N^{\alpha\beta h}) + \int_{\Omega} (\kappa_{\alpha\beta} - \kappa_{\alpha\beta}^h)(M^{\alpha\beta} - M^{\alpha\beta h}) \right) d\Omega}}{\sqrt{\int_{\Omega} (\varepsilon_{\alpha\beta} N^{\alpha\beta} + \kappa_{\alpha\beta} M^{\alpha\beta}) d\Omega}}
 \end{aligned}
 \tag{61}$$

### 327 5.1. Patch tests

328 The linear and quadratic patch tests for flat and curved thin shells are firstly  
 329 studied to verify the variational consistency of the proposed method. As shown  
 330 in Fig. 3, the flat and curved models are depicted by an identical parametric  
 331 domain  $\Omega = (0, 1) \otimes (0, 1)$ , where the cylindrical coordinate system with radius  
 332  $R = 1$  is employed to describe the curved model, and the whole domain  $\Omega$   
 333 is discretized by the 165 meshfree nodes. All the boundaries are enforced as  
 334 essential boundary conditions with the following manufactured exact solution:

$$\mathbf{v} = \begin{Bmatrix} (\xi^1 + 2\xi^2)^n \\ (3\xi^1 + 4\xi^2)^n \\ (5\xi^1 + 6\xi^2)^n \end{Bmatrix}, \quad n = \begin{cases} 1 & \text{Linear patch test} \\ 2 & \text{Quadratic patch test} \end{cases}
 \tag{62}$$

335 Table 1 lists the  $L_2$ - and  $H_e$ -Error results of patch test with flat model, where  
 336 the RKGSI scheme with variational consistent essential boundary enforcement,  
 337 i.e. RKGSI-Nitsche and RKGSI-HW, can pass the linear and quadratic patch  
 338 test. Due to the loss of variational consistency condition, even with Nitsche's  
 339 method, Gauss meshfree formulations show noticeable errors. Table 2 shows  
 340 the results for curved model, which indicated that all the considered methods  
 341 cannot pass the patch test. This is mainly because the proposed smoothed  
 342 gradient of Eqs. (35) and (36) could not exactly reproduce the non-polynomial  
 343 membrane and bending stress. However, the RKGSI-HW and RKGSI-Nitsche  
 344 methods also provide better accuracy compared to others due to the fulfillment

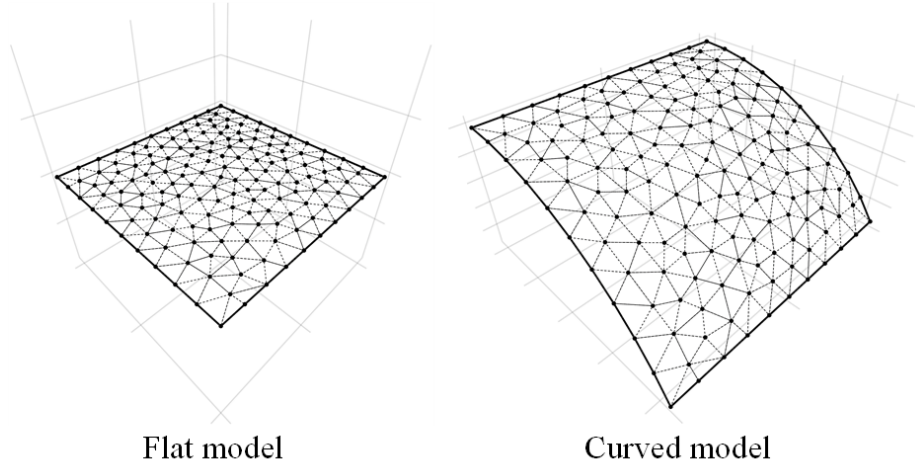


Figure 3: Meshfree discretization for patch test

345 of first second-order variational consistency. Meanwhile, the bending moment  
 346 contours of  $M^{12}$  are listed in Fig. 4, which further verify that the proposed  
 347 method provided a satisfactory result compared to exact solution. On the other  
 348 hand, the conventional Gauss meshree formulations showed errors.

Table 1: Results of patch test for flat model.

	Linear patch test		Quadratic patch test	
	$L_2$ -Error	$H_e$ -Error	$L_2$ -Error	$H_e$ -Error
GI-Penalty	$4.45E-4$	$1.35E-2$	$2.01E-3$	$1.63E-2$
GI-Nitsche	$4.51E-4$	$1.42E-2$	$1.22E-3$	$1.68E-2$
RKGSi-Penalty	$3.64E-9$	$6.77E-8$	$4.54E-9$	$6.57E-8$
RKGSi-Nitsche	$3.31E-12$	$1.34E-11$	$5.98E-12$	$1.21E-11$
RKGSi-HR	$6.67E-13$	$1.50E-11$	$1.07E-12$	$1.26E-11$

Table 2: Results of patch test for cylindrical model.

	Linear patch test		Quadratic patch test	
	$L_2$ -Error	$H_e$ -Error	$L_2$ -Error	$H_e$ -Error
GI-Penalty	$3.79E-4$	$1.30E-2$	$1.74E-3$	$1.37E-2$
GI-Nitsche	$4.04E-4$	$1.42E-2$	$1.15E-3$	$1.49E-2$
RKGSi-Penalty	$1.47E-4$	$5.39E-3$	$2.26E-4$	$2.09E-3$
RKGSi-Nitsche	$2.41E-6$	$7.37E-5$	$2.47E-6$	$2.89E-5$
RKGSi-HR	$4.28E-6$	$1.30E-4$	$9.69E-6$	$2.41E-4$

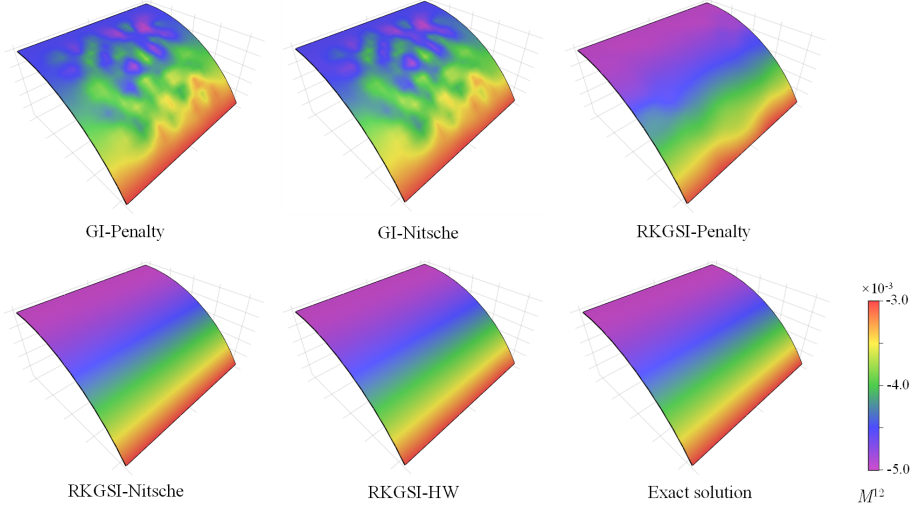


Figure 4: Contour plots of  $M^{12}$  for curved shell patch test.

### 5.2. Scordelis-Lo roof

This example considers the classical Scordelis-Lo roof problem, as depicted in Fig. 5. The cylindrical roof has dimensions  $R = 25$ ,  $L = 50$ ,  $h = 0.25$ , Young's modulus  $E = 4.32 \times 10^8$  and Poisson's ratio  $\nu = 0.0$ . The entire roof is subjected to a uniform body force of  $b_z = -90$ , with the straight edges remaining free and the curved edges are enforced by  $v_x = v_z = 0$ .

Due to the symmetry, only a quadrant of the model is considered for meshfree analysis, which is discretized by the  $11 \times 16$ ,  $13 \times 20$ ,  $17 \times 24$  and  $19 \times 28$  meshfree nodes, as listed in Fig. 6. The comparison of the displacement in  $z$ -direction at node  $A$ ,  $v_{A3}$ , is used as the investigated quantity, with the reference value  $0.3024$  given by [32]. Firstly, Fig. 7 presents a sensitivity study for the artificial parameters of  $\alpha_v$ 's,  $\alpha_\theta$ 's in the RKGSI meshfree formulations with Nitsche's method and penalty method. The results of Fig. 7 revealed, Nitsche's method observed less artificial sensitivity. However, both the methods cannot trivially determine the optimal values of the artificial parameters. The optimal artificial parameters from Fig. 7 are adopted for the convergence study in Fig. 8. The convergence result showed that the RKGSI get satisfactory results while the traditional Gauss methods demonstrated noticeable errors.

### 5.3. Pinched Hemispherical shell

Consider the hemispherical shell shown in Fig. 9, which is loaded at four points  $P = \pm 2$  at  $90^\circ$  interval at its bottom. The hemispherical shell has a radius  $R = 10$ , thickness  $h = 0.04$ , Young's modulus  $E = 6.825 \times 10^7$  and Poisson's ratio  $\nu = 0.3$ .

Due to symmetry, only quadrant model, where the  $8 \times 8$ ,  $16 \times 16$ ,  $24 \times 24$  and  $32 \times 32$  meshfree nodes have been discretized, was considered. The quantity

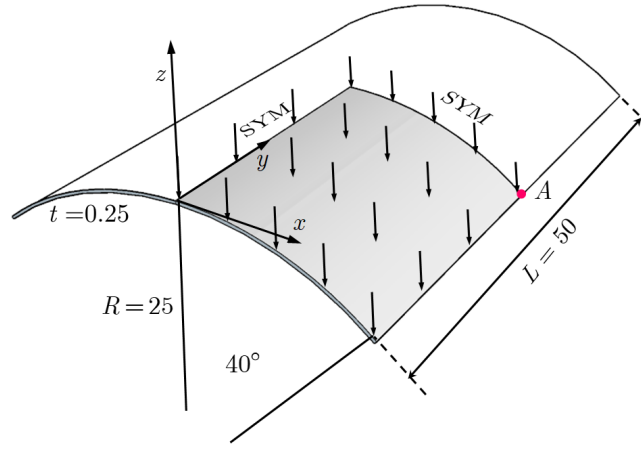


Figure 5: Description of Scordelis-Lo roof problem.

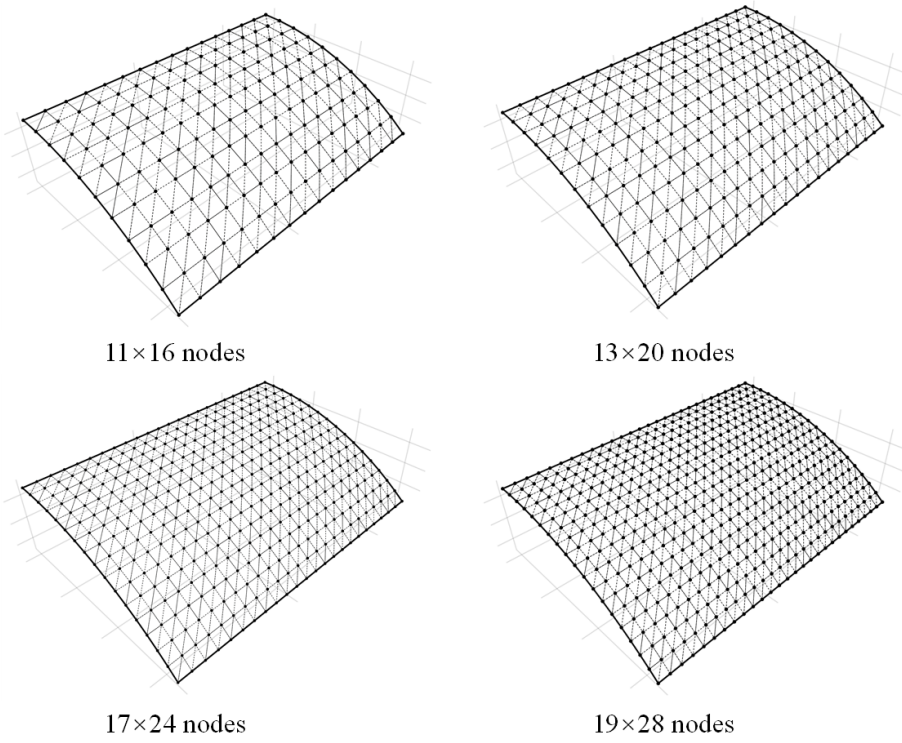


Figure 6: Meshfree discretizations for Scordelis-Lo roof problem.

374 under investigation for convergence is the displacement at  $x$ -direction on point

375  $A, v_{A1}$ . Fig. 10 displays the corresponding convergence results, indicating the  
 376 RKGSi scheme performed significantly better compared to the GI meshfree for-  
 377 mulation. Meanwhile, the efficiency comparison for this problem is also shown  
 378 in Fig. 11, in which the CPU time for assembly and calculation of shape func-  
 379 tions are considered. Fig. 11(a) indicates that the RKGSi scheme observed  
 380 high efficiency in assembly. This is due to the variational inconsistent Gauss  
 381 meshfree formulation which require more Gaussian points to get satisfactory  
 382 results. Fig. 11(b) lists the CPU time spent on enforcing essential boundary  
 383 conditions for the penalty method, Nitsche's method and proposed HW method.  
 384 The results highlighted that the proposed HW method consumed comparable  
 385 CPU time in assembly compared to Nitsche's method. However, less time was  
 386 spent to calculate the shape functions. Since both the HW method and penalty  
 387 method were developed considering the shape functions first order derivatives.  
 388 For this reason, both the methods shared an almost identical time in computing  
 389 the shape functions.

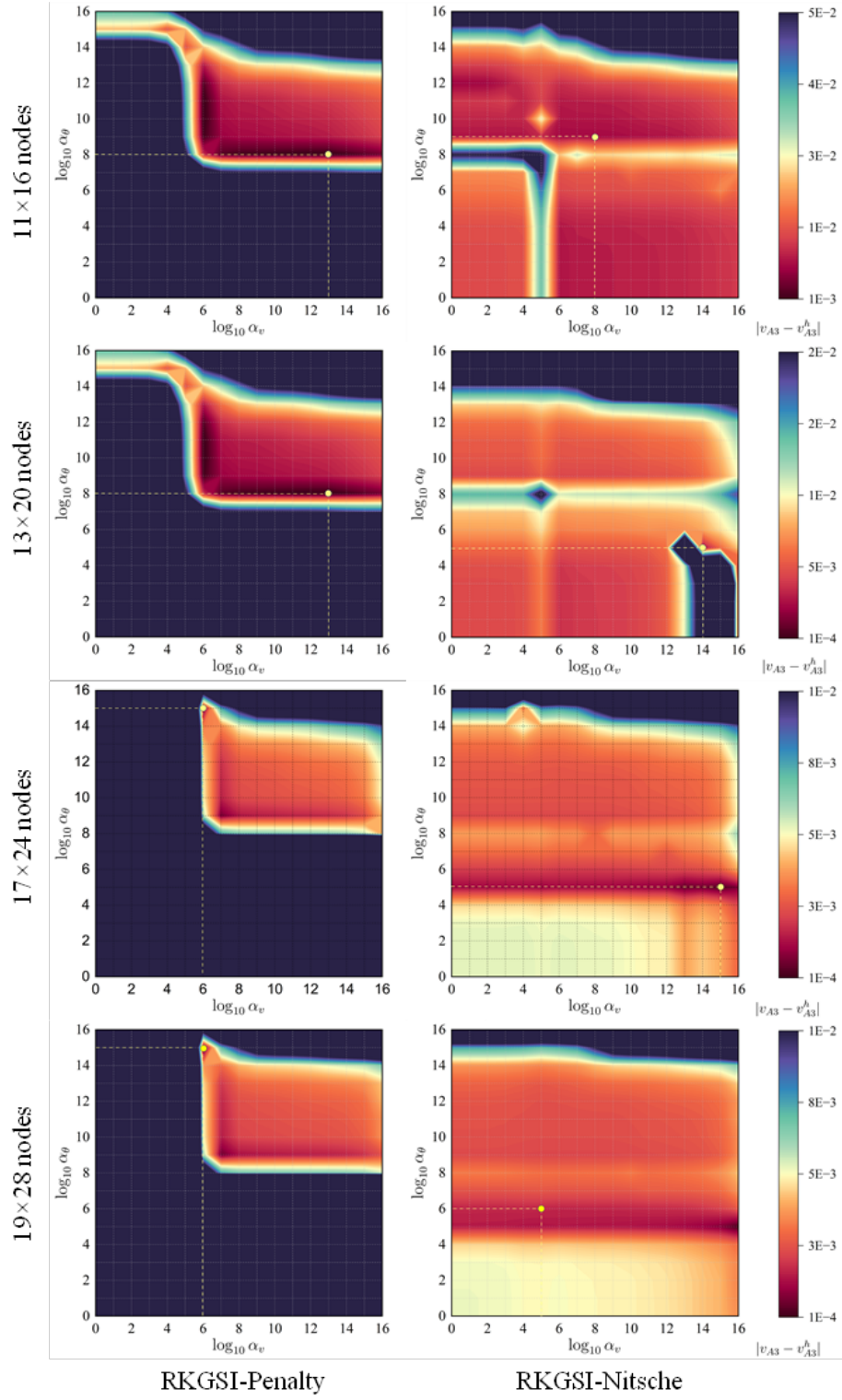


Figure 7: Sensitivity comparison of  $\alpha_v$  and  $\alpha_\theta$  for Scordelis-Lo problem.



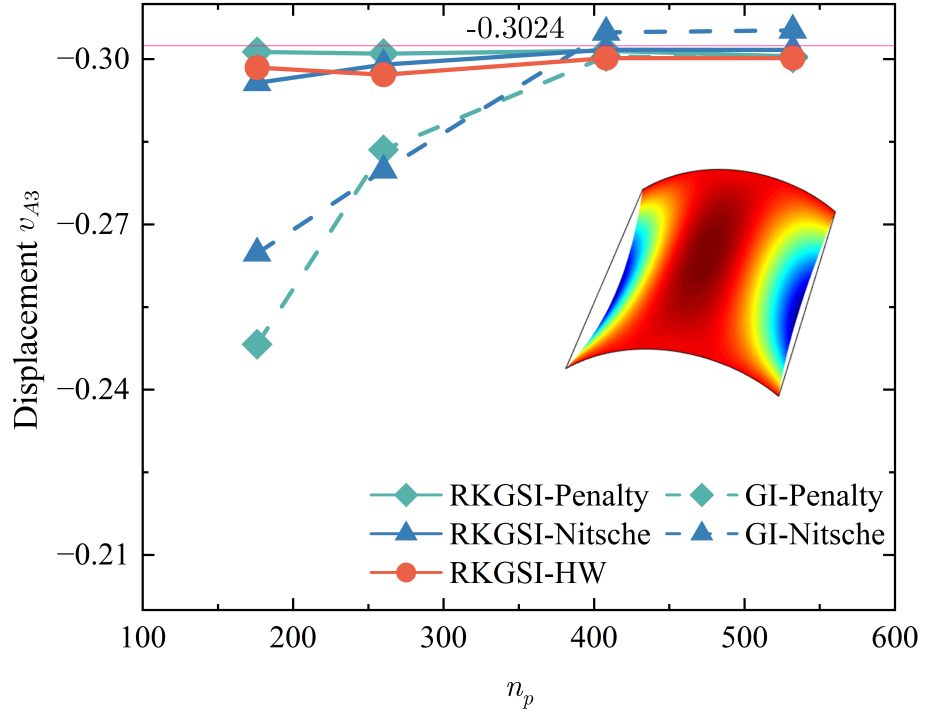


Figure 8: Displacement convergence for Scordelis-Lo roof problem.

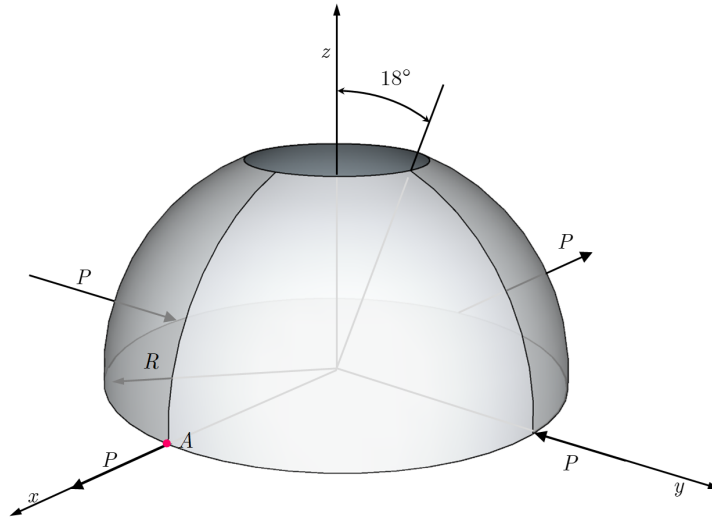


Figure 9: Description of pinched hemispherical shell problem.

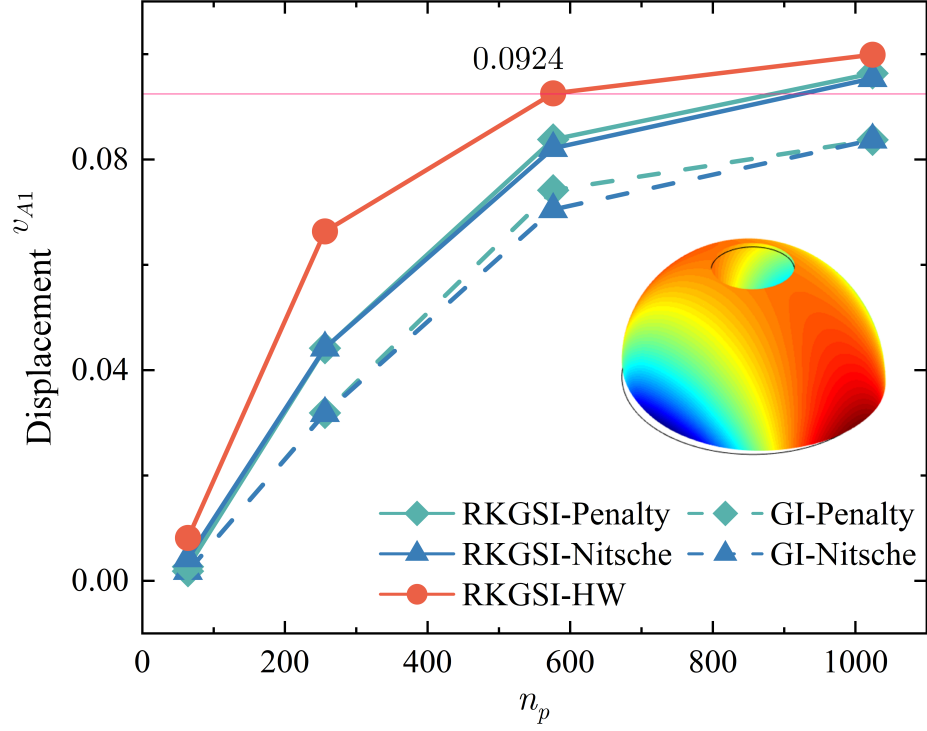


Figure 10: Displacement convergence for pinched hemispherical shell problem.

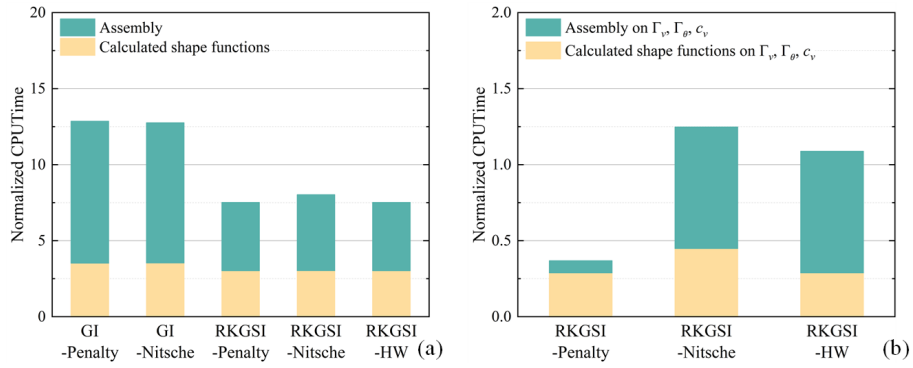


Figure 11: efficiency comparison for pinched hemispherical shell problem: (a) Whole domain; (b) Essential boundaries

## 6. Conclusion

In this study, an efficient and quasi-consistent meshfree thin shell formulation was presented to naturally enforce the essential boundary conditions. Mixed formulation with the Hu-Washizu principle weak form is adopted, where the traditional meshfree shape functions discretized the displacement, and the strains and stresses were expressed by the reproducing kernel smoothed gradients and the covariant smoothed gradients, respectively. The smoothed gradient naturally embedded the first second-order integration constraints and has a quasi variational consistency for the curved models in each integration cell. Owing to the Hu-Washizu variational principle, the essential boundary condition enforcement has a similar form with the conventional Nitsche's method; both have consistent and stabilized terms. The costly high order derivatives in the Nitsche's consistent term have been replaced by the smoothed gradients, which improved the computational speed due to the reproducing kernel gradient smoothing framework. Furthermore, the stabilized term naturally existed in the Hu-Washizu weak form, and the artificial parameter needed in Nitsche's stabilized term has vanished, which can automatically maintain the coercivity for the stiffness matrix. The numerical results demonstrated that the proposed Hu-Washizu quasi-consistent meshfree thin shell formulation showed excellent accuracy, efficiency, and stability.

**Acknowledgment**

The support of this work by the National Natural Science Foundation of China (12102138, 52350410467) and the Natural Science Foundation of Fujian Province of China (2023J01108, 2022J05056) is gratefully acknowledged.

## 414 Appendix A. Green's theorems for in-plane vector

415 This Appendix discusses two kinds of Green's theorems used for the devel-  
 416 opment of the proposed meshfree method. For an arbitrary vectors  $v^\alpha$  and a  
 417 scalar function  $f$ , with Green's theorem for in-plane vector, the first Green's  
 418 theorem is listed as follows [30]:

$$\begin{aligned} \int_{\Omega} f_{,\alpha} v^\alpha d\Omega &= \int_{\Gamma} f v^\alpha n_\alpha d\Gamma - \int_{\Omega} f (v_{,\alpha}^\alpha + \Gamma_{\beta\alpha}^\beta v^\alpha) d\Omega \\ &= \int_{\Gamma} f v^\alpha n_\alpha d\Gamma - \int_{\Omega} f v^\alpha|_\alpha d\Omega \end{aligned} \quad (\text{A.1})$$

419 where  $\Gamma_{\alpha\beta}^\gamma = \mathbf{a}_{\alpha,\beta} \cdot \mathbf{a}^\gamma$  denotes the Christoffel symbol of the second kind.  $v^\alpha|_\alpha$   
 420 can be represented as the in-plane covariant derivative of the vector  $v^\alpha$ :

$$v^\alpha|_\alpha = v_{,\alpha}^\alpha + \Gamma_{\beta\alpha}^\beta v^\alpha \quad (\text{A.2})$$

421 The second Green's theorem is established with a mixed form of second  
 422 order derivative. Let  $A^{\alpha\beta}$  can be an arbitrary symmetric second order tensor,  
 423 the Green's theorem yields [30]:

$$\begin{aligned} \int_{\Omega} f_{,\alpha}|_\beta A^{\alpha\beta} d\Omega &= \int_{\Gamma} f_{,\gamma} n^\gamma A^{\alpha\beta} n_\alpha n_\beta d\Gamma - \int_{\Gamma} f (A^{\alpha\beta} s_\alpha n_\beta)_{,\gamma} s^\gamma d\Gamma + [[f A^{\alpha\beta} s_\alpha n_\beta]]_{\mathbf{x} \in C} \\ &\quad - \int_{\Gamma} f (A_{,\beta}^{\alpha\beta} n_\alpha + \Gamma_{\alpha\beta}^\gamma A^{\alpha\beta} n_\gamma + \Gamma_{\gamma\beta}^\gamma A^{\alpha\beta} n_\alpha) d\Gamma \\ &\quad + \int_{\Omega} f \left( \Gamma_{\alpha\beta,\gamma}^\gamma A^{\alpha\beta} + \Gamma_{\alpha\beta}^\gamma A_{,\gamma}^{\alpha\beta} + \Gamma_{\eta\gamma}^\eta \Gamma_{\alpha\beta}^\gamma A^{\alpha\beta} \right. \\ &\quad \left. + A_{,\alpha\beta}^{\alpha\beta} + \Gamma_{\gamma\beta,\alpha}^\gamma A^{\alpha\beta} + 2\Gamma_{\gamma\alpha}^\gamma A_{,\beta}^{\alpha\beta} + \Gamma_{\gamma\alpha}^\gamma \Gamma_{\eta\beta}^\eta A^{\alpha\beta} \right) d\Omega \\ &= \int_{\Gamma} f_{,\gamma} n^\gamma A^{\alpha\beta} n_\alpha n_\beta d\Gamma - \int_{\Gamma} f (A^{\alpha\beta} s_\alpha n_\beta)_{,\gamma} s^\gamma d\Gamma + [[f A^{\alpha\beta} s_\alpha n_\beta]]_{\mathbf{x} \in C} \\ &\quad - \int_{\Gamma} f A^{\alpha\beta}|_\beta n_\alpha d\Gamma + \int_{\Omega} f A^{\alpha\beta}|_{\alpha\beta} d\Omega \end{aligned} \quad (\text{A.3})$$

424 with

$$A^{\alpha\beta}|_\beta = A_{,\beta}^{\alpha\beta} + \Gamma_{\beta\gamma}^\alpha A^{\beta\gamma} + \Gamma_{\gamma\beta}^\gamma A^{\alpha\beta} \quad (\text{A.4})$$

425

$$\begin{aligned} A^{\alpha\beta}|_{\alpha\beta} &= \Gamma_{\alpha\beta,\gamma}^\gamma A^{\alpha\beta} + \Gamma_{\alpha\beta}^\gamma A_{,\gamma}^{\alpha\beta} + \Gamma_{\eta\gamma}^\eta \Gamma_{\alpha\beta}^\gamma A^{\alpha\beta} \\ &\quad + A_{,\alpha\beta}^{\alpha\beta} + \Gamma_{\gamma\beta,\alpha}^\gamma A^{\alpha\beta} + 2\Gamma_{\gamma\alpha}^\gamma A_{,\beta}^{\alpha\beta} + \Gamma_{\gamma\alpha}^\gamma \Gamma_{\eta\beta}^\eta A^{\alpha\beta} \end{aligned} \quad (\text{A.5})$$

426 For the sake of brevity, the notion of covariant derivative is extended to a  
 427 scalar function as:

$$f|_\alpha = f_{,\alpha} + \Gamma_{\beta\alpha}^\beta f \quad (\text{A.6})$$

428

$$f|_\beta n_\alpha = f_{,\beta} n_\alpha + \Gamma_{\alpha\beta}^\gamma f n_\gamma + \Gamma_{\gamma\beta}^\gamma f n_\alpha \quad (\text{A.7})$$

429

$$\begin{aligned} f|_{\alpha\beta} &= \Gamma_{\alpha\beta,\gamma}^\gamma f + \Gamma_{\alpha\beta}^\gamma f_{,\gamma} + \Gamma_{\eta\gamma}^\eta \Gamma_{\alpha\beta}^\gamma f \\ &\quad + f_{,\alpha\beta} + \Gamma_{\gamma\beta,\alpha}^\gamma f + 2\Gamma_{\gamma\alpha}^\gamma f_{,\beta} + \Gamma_{\gamma\alpha}^\gamma \Gamma_{\eta\beta}^\eta f \end{aligned} \quad (\text{A.8})$$

430 **Appendix B. Derivations for stiffness metrics and force vectors**

431 This Appendix details the derivations of stiffness matrices and force vectors  
 432 in Eqs. (53)-(55), where the relationships of Eqs. (40), (41), (44) and (46) are  
 433 used herein. Firstly, the membrane strain terms are considered as follows:

$$\begin{aligned}
 & \sum_{C=1}^{n_e} \int_{\Omega_C} \delta \tilde{\varepsilon}_{\alpha\beta}^h h C^{\alpha\beta\gamma\eta} \tilde{\varepsilon}_{\gamma\eta}^h d\Omega \\
 &= \sum_{C=1}^{n_e} \sum_{I,J=1}^{n_p} \delta \mathbf{d}_I \cdot \underbrace{\int_{\Omega_C} \tilde{\varepsilon}_{\alpha\beta I} h C^{\alpha\beta\gamma\eta} \mathbf{a}_\gamma \mathbf{q}^T d\Omega \mathbf{G}^{-1} \bar{\mathbf{g}}_{\eta J}}_{\tilde{\mathbf{g}}_I^{\eta T}} \cdot \mathbf{d}_J \\
 &= \sum_{C=1}^{n_e} \sum_{I,J=1}^{n_p} \delta \mathbf{d}_I \cdot \int_{\Gamma_C \cap \Gamma_v} \Psi_J \underbrace{\mathbf{q}^T \mathbf{G}^{-1} \tilde{\mathbf{g}}_I^\alpha n_\alpha}_{\tilde{\mathbf{T}}_{NI}} d\Gamma \cdot \mathbf{d}_J \\
 &= \sum_{I,J=1}^{n_p} \delta \mathbf{d}_I \cdot \int_{\Gamma_v} \tilde{\mathbf{T}}_{NI} \Psi_J d\Gamma \cdot \mathbf{d}_J
 \end{aligned} \tag{B.1}$$

434 with

$$435 \quad \tilde{\mathbf{g}}_I^\alpha = \mathbf{q} \mathbf{a}_\beta h C^{\alpha\beta\gamma\eta} \tilde{\varepsilon}_{\alpha\beta I} \tag{B.2}$$

$$436 \quad \tilde{\mathbf{T}}_{NI} = \mathbf{q}^T \mathbf{G}^{-1} \tilde{\mathbf{g}}_I^\alpha n_\alpha \tag{B.3}$$

Following this path, the bending strain terms can be reorganized by:

$$\begin{aligned}
 & \sum_{C=1}^{n_e} \int_{\Omega_C} \delta \tilde{\kappa}_{\alpha\beta}^h \frac{h^3}{12} C^{\alpha\beta\gamma\eta} \tilde{\kappa}_{\gamma\eta}^h d\Omega \\
 &= \sum_{C=1}^{n_e} \sum_{I,J=1}^{n_p} \delta \mathbf{d}_I \cdot \underbrace{\int_{\Omega_C} \tilde{\kappa}_{\alpha\beta I} \frac{h^3}{12} C^{\alpha\beta\gamma\eta} \mathbf{a}_3 \mathbf{q}^T d\Omega \mathbf{G}^{-1} \bar{\mathbf{g}}_{\gamma\eta J}}_{\tilde{\mathbf{g}}_I^{\gamma\eta T}} \cdot \mathbf{d}_J \\
 &= \sum_{C=1}^{n_e} \sum_{I,J=1}^{n_p} \delta \mathbf{d}_I \cdot \left( \begin{aligned} & \int_{\Gamma_C \cap \Gamma_\theta} \underbrace{\mathbf{q}^T \mathbf{G}^{-1} \tilde{\mathbf{g}}_I^{\alpha\beta} n_\alpha n_\beta}_{\tilde{\mathbf{M}}_{nnI}} n^\gamma \Psi_{J,\gamma} d\Gamma \\ & - \int_{\Gamma_C \cap \Gamma_v} \underbrace{(\mathbf{q}_{|\beta}^T \mathbf{G}^{-1} \tilde{\mathbf{g}}_I^{\alpha\beta} n_\alpha + (\mathbf{q}^T \mathbf{G}^{-1} \tilde{\mathbf{g}}_I^{\alpha\beta} s_\alpha n_\beta)_{,\gamma} s^\gamma)}_{\tilde{\mathbf{T}}_{MI}} \Psi_J d\Gamma \\ & + \underbrace{[\mathbf{q}^T \mathbf{G}^{-1} \tilde{\mathbf{g}}_I^{\alpha\beta} s_\alpha n_\beta \Psi_J]}_{\tilde{\mathbf{P}}_I \mathbf{a}_3} \Big|_{\mathbf{x} \in C_C \cap C_v} \end{aligned} \right) \cdot \mathbf{d}_J \\
 &= \sum_{I,J=1}^{n_p} \delta \mathbf{d}_I \cdot \left( \int_{\Gamma_\theta} \tilde{\mathbf{M}}_{nnI} n^\gamma \Psi_{J,\gamma} d\Gamma - \int_{\Gamma_v} \tilde{\mathbf{T}}_{MI} \Psi_J d\Gamma + [[\tilde{\mathbf{P}}_I \Psi_J]]_{\mathbf{x} \in C_v} \right)
 \end{aligned} \tag{B.4}$$

437 with

$$\tilde{\mathbf{g}}_I^{\alpha\beta} = \int_{\Omega_C} \mathbf{q} \frac{h^3}{12} C^{\alpha\beta\gamma\eta} \mathbf{a}_3 \tilde{\boldsymbol{\kappa}}_{\alpha\beta I} d\Omega \quad (\text{B.5})$$

438

$$\begin{cases} \tilde{M}_{nnI} = \mathbf{q}^T \mathbf{G}^{-1} \tilde{\mathbf{g}}_I^{\alpha\beta} n_\alpha n_\beta \\ \tilde{\mathbf{T}}_{MI} = \mathbf{q}_{|\beta}^T \mathbf{G}^{-1} \tilde{\mathbf{g}}_I^{\alpha\beta} n_\alpha + (\mathbf{q}^T \mathbf{G}^{-1} \tilde{\mathbf{g}}_I^{\alpha\beta} s_\alpha n_\beta)_{,\gamma} s^\gamma \\ \tilde{\mathbf{P}}_I = \mathbf{q}^T \mathbf{G}^{-1} \tilde{\mathbf{g}}_I^{\alpha\beta} s_\alpha n_\beta \cdot \mathbf{a}_3 \end{cases} \quad (\text{B.6})$$

## References

- [1] L. H. Donnell, Beams, Plates and Shells, McGraw-Hill. `arXiv:0_IeAQAAIAAJ`.
- [2] T. J. Hughes, The Finite Element Method: Linear Static and Dynamic Finite Element Analysis, Dover Publications.
- [3] T. Belytschko, Y. Y. Lu, L. Gu, Element-free Galerkin methods 37 (2) 229–256. `arXiv:10208278`.
- [4] W. K. Liu, S. Jun, Y. F. Zhang, Reproducing kernel particle methods 20 (8-9) 1081–1106.
- [5] J. S. Chen, M. Hillman, S. W. Chi, Meshfree methods: Progress made after 20 years 143 (4) 04017001.
- [6] P. Krysl, T. Belytschko, Analysis of thin shells by the Element-Free Galerkin method 33 (20) 3057–3080.
- [7] G. R. Liu, Meshfree Methods: Moving Beyond the Finite Element Method, Second Edition, Crc Press.
- [8] X. Zhang, K. Z. Song, M. W. Lu, X. Liu, Meshless methods based on collocation with radial basis functions 26 333–343.
- [9] D. Millán, A. Rosolen, M. Arroyo, Thin shell analysis from scattered points with maximum-entropy approximants 85 (6) 723–751.
- [10] L. Wang, M. Hu, Z. Zhong, F. Yang, Stabilized Lagrange Interpolation Collocation Method: A meshfree method incorporating the advantages of finite element method 404 115780.
- [11] P. Suchde, T. Jacquemin, O. Davydov, Point Cloud Generation for Mesh-free Methods: An Overview 30 (2) 889–915.
- [12] L. Deng, D. Wang, An accuracy analysis framework for meshfree collocation methods with particular emphasis on boundary effects 404 115782.
- [13] S. Fernández-Méndez, A. Huerta, Imposing essential boundary conditions in mesh-free methods 193 (12-14) 1257–1275.
- [14] X. Li, Error estimates for the moving least-square approximation and the element-free Galerkin method in n-dimensional spaces 99 77–97.
- [15] J. Wu, D. Wang, An accuracy analysis of Galerkin meshfree methods accounting for numerical integration 375 113631.
- [16] J.-S. Chen, H.-P. Wang, New boundary condition treatments in meshfree computation of contact problems 187 (3) 441–468.



- 473 [17] D. Liu, Y. M. Cheng, The interpolating element-free Galerkin (IEFG)  
474 method for three-dimensional potential problems 108 115–123.
- 475 [18] V. Ivannikov, C. Tiago, P. M. Pimenta, On the boundary conditions of the  
476 geometrically nonlinear Kirchhoff–Love shell theory 51 (18) 3101–3112.
- 477 [19] Y. Y. Lu, T. Belytschko, L. Gu, A new implementation of the element free  
478 Galerkin method 113 (3-4) 397–414. [arXiv:26071039](#).
- 479 [20] T. Zhu, S. N. Atluri, A modified collocation method and a penalty formu-  
480 lation for enforcing the essential boundary conditions in the element free  
481 Galerkin method 21 (3) 211–222.
- 482 [21] S. Skatulla, C. Sansour, Essential boundary conditions in meshfree methods  
483 via a modified variational principle: Applications to shell computations  
484 15 (2) 123–142.
- 485 [22] J. S. Chen, C. T. Wu, S. Yoon, Y. You, A stabilized conforming nodal  
486 integration for Galerkin mesh-free methods 50 (2) 435–466.
- 487 [23] J. S. Chen, M. Hillman, M. Rüter, An arbitrary order variationally con-  
488 sistent integration for Galerkin meshfree methods 95 (5) 387–418. [arXiv:](#)  
489 [260949200001](#).
- 490 [24] Q. Duan, X. Li, H. Zhang, T. Belytschko, Second-order accurate derivatives  
491 and integration schemes for meshfree methods 92 (4) 399–424. [arXiv:](#)  
492 [260949200001](#).
- 493 [25] D. Wang, J. Wu, An inherently consistent reproducing kernel gradient  
494 smoothing framework toward efficient Galerkin meshfree formulation with  
495 explicit quadrature 349 628–672.
- 496 [26] J. Wang, X. Ren, A consistent projection integration for Galerkin meshfree  
497 methods 414 116143.
- 498 [27] J. Wu, X. Wu, Y. Zhao, D. Wang, A consistent and efficient method for  
499 imposing meshfree essential boundary conditions via hellinger-reissner vari-  
500 ational principle. 54 (12) 3283–3296.
- 501 [28] J. Wu, X. Wu, Y. Zhao, D. Wang, A rotation-free Hellinger-Reissner mesh-  
502 free thin plate formulation naturally accommodating essential boundary  
503 conditions 154 122–140.
- 504 [29] H. Dah-wei, A method for establishing generalized variational principle  
505 6 (6) 501–509.
- 506 [30] J. Benzaken, J. A. Evans, S. F. McCormick, R. Tamstorf, Nitsche’s method  
507 for linear Kirchhoff–Love shells: Formulation, error analysis, and verifica-  
508 tion 374 113544.

- 509 [31] H. Du, J. Wu, D. Wang, J. Chen, A unified reproducing kernel gradient  
510 smoothing Galerkin meshfree approach to strain gradient elasticity 70 (1)  
511 73–100.
- 512 [32] R. H. Macneal, R. L. Harder, A proposed standard set of problems to test  
513 finite element accuracy 1 (1) 3–20.